Report
**R-19-13**
May 2019

# Modelling of concrete degradation in a one-million-year perspective – Hydro-chemical processes

## Report for the safety evaluation SE-SFL

**Andrés Idiart**
**Marcelo Laviña**

SVENSK KÄRNBRÄNSLEHANTERING AB

SWEDISH NUCLEAR FUEL
AND WASTE MANAGEMENT CO

Box 3091, SE-169 03 Solna
Phone +46 8 459 84 00
skb.se

SVENSK KÄRNBRÄNSLEHANTERING

ISSN 1402-3091
**SKB R-19-13**
ID 1581165
May 2019

# Modelling of concrete degradation in a one-million-year perspective – Hydro-chemical processes

## Report for the safety evaluation SE-SFL

Andrés Idiart, Marcelo Laviña
Amphos 21 Consulting S.L.

# Summary

A 1D reactive transport model has been used for simulations of concrete degradation in BHK, a rock vault in the proposed repository concept for long-lived low and intermediate level waste (SFL). A software interface between Comsol Multiphysics and Phreeqc (iCP) has been used in the modelling. The focus has been on evaluating the pH, porosity, effective diffusivity and hydraulic conductivity of the BHK concrete backfill over 1-million-year time span. The time-evolution of these parameters serves as input to the radionuclide transport model used in the SFL safety evaluation. In addition, the results from concrete degradation simulations in 1D have been compared to equivalent simulations in 2D, as well as to analytical expressions based on the shrinking core model.

# Sammanfattning

En reaktiv transportmodell i 1D har använts för att simulera betongdegradering i BHK, en bergssal i det föreslagna förvarskonceptet för långlivat låg- och medelaktivt avfall. Ett mjukvaruinterface mellan Comsol Multiphysics och Phreeqc (iCP) har använts vid modelleringen. Fokus har varit på att utvärdera pH, porositet, effektiv diffusivitet och hydraulisk konduktivitet i betongåterfyllnaden i BHK, sett över en miljon år. Tidsutvecklingen av dessa parametrar blir indata till radionuklidtransportmodellen som används i säkerhetsvärderingen för SFL. Vidare har resultat från simuleringar av betongdegradering i 1D jämförts med en motsvarande simuleringar i 2D och även med resultat från analytiska shrinking core modeller.

# Contents

# 1 Introduction

SKB plans to dispose of long-lived low and intermediate level waste (LILW) in a deep geological repository, named SFL. The total capacity of SFL is estimated to approximately 16 000 $m^3$. About one third of the waste originates from nuclear power plants in the form of neutron-irradiated components and control rods. The remainder comes from AB SVAFO and Studsvik Nuclear AB, who manage the legacy waste and the waste from hospitals, industry and research. Possible repository concepts for SFL have been evaluated and Elfwing et al. (2013) proposed a repository concept to be analysed in an evaluation of post-closure safety (SE-SFL). This study focusses on the repository concept for metallic waste, denoted BHK. The main components of the engineered barrier system are shown in Figure 1-1. A repository structure containing the waste will be made of reinforced concrete with a thickness of ~0.5 m. The waste is segmented, after which the parts are deposited in steel tanks and stabilized with grout. The steel tanks are emplaced in the repository.

The BHK vault will be backfilled with concrete, which acts as a barrier against groundwater flow and contributes to a low diffusion rate and high sorption of many radionuclides. The concrete in the barrier will furthermore create an alkaline environment, reducing the corrosion rate of steel and thus limiting the release rate of radionuclides.

In previous work, long-term performance of concrete barriers in the BHK vault as a result of interaction with groundwater has been assessed by means of 2D and 3D reactive transport models (Idiart and Shafei 2019). These models included groundwater flow, chemical reactions within the concrete barriers, and physical degradation of the concrete barriers, i.e. flow and transport properties. The simulation time considered was 100 000 years at the most, limited by the computational effort.

The present work aims to address concrete degradation and long-term performance of BHK over 1 million years, using a one-dimensional (1D) reactive transport model. Mass transport by advection and diffusion is coupled to chemical reactions using iCP (Nardi et al. 2014). This approach explicitly takes into account the feedback between chemically-induced porosity changes and flow and transport properties.

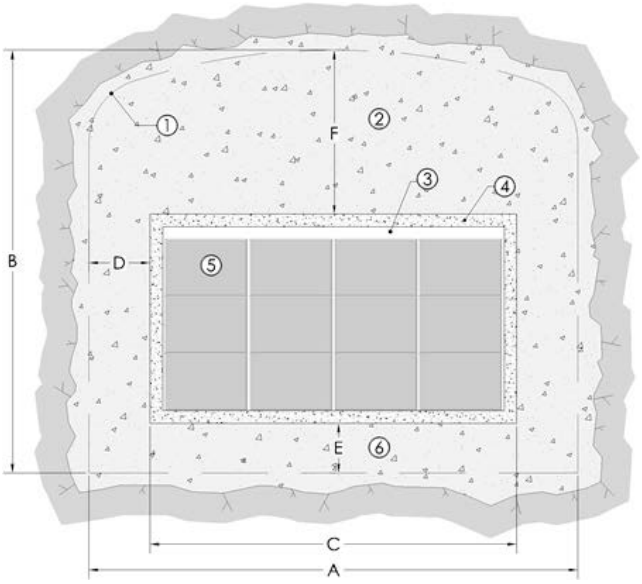


***Figure 1-1.*** *Schematic cross-sectional layout of the BHK vault for metallic waste (from Elfwing et al. 2013). Legend: 1.) Theoretical tunnel contour. 2) Concrete backfill. 3) Grout. 4) Concrete structure. (0.5 m). 5) Steel tanks. 6) Concrete. Approximate dimensions: A = 20.6 m, B = 19.6 m, C = 15 m, D = 2.8 m, E = 2.4 m, F = 8.8 m.*

# 2 Objectives and scope

The main objective of the present study is to provide an estimation of the long-term evolution of the key parameters of the concrete backfill of the BHK vault in SFL over a period of 1 million years. These indicators consist of the pH of the pore solution, the porosity of concrete, and the effective diffusivity and hydraulic conductivity of the backfill. A software interface between Comsol Multiphysics (COMSOL 2015) and Phreeqc (Parkhurst and Appelo 2013), named iCP, has been used in the modelling (Nardi et al. 2014).

The numerical analysis presented here is limited to 1D reactive transport processes in the concrete backfill, with groundwater flow conditions representative of the expected horizontal flow across the backfill at the left of the waste domain. The conceptual model is based on the Base Case (Case I) presented in Idiart and Shafei (2019). A comparison with analytical solutions based on the shrinking core model (Levenspiel 1972) and with previously obtained results of a 2D reactive transport model (Idiart and Shafei 2019) is also presented.

# 3 Methodology

Concrete degradation in BHK is mainly driven by groundwater interaction. To capture this, a 1D reactive transport model of the BHK concrete backfill has been developed and implemented in iCP (Nardi et al. 2014). The model considers the coupling between chemical reactions and advective/ diffusive solute transport. The chemical setup in terms of groundwater, porewater and mineralogical compositions is identical to the Base Case (Case I), presented in Idiart and Shafei (2019).

A 3D representation of the BHK vault is shown in Figure 3-1. The geometry is divided into a set of control volumes, as proposed in the modelling of the near-field hydrology (Abarca et al. 2019). In the context of the present work, the control volumes represent material domains. The concrete backfill is divided into an outer and an inner zone. In addition, a control volume for the waste is defined.

The total thickness of the concrete backfill at the sides of the waste is 2.8 m (see Figure 1-1). The thickness of the outer and inner backfill control volumes are here 1.4 m each. The concrete structure together with the grouted waste inside is considered as one homogeneous domain. The concrete material domains of BHK are thus the following:

- Outer concrete backfill
- Inner concrete backfill
- Waste

As described in Chapter 4, the 1D model developed in this work has a length of 2.8 m, corresponding to the thickness of the concrete backfill at the left side of the waste domain.

The radionuclide transport model used in the SFL safety evaluation requires the following time-dependent properties for concrete for the outer and inner backfill:

- pH
- Porosity
- Effective diffusivity ($m^2/s$)
- Hydraulic conductivity (m/s)

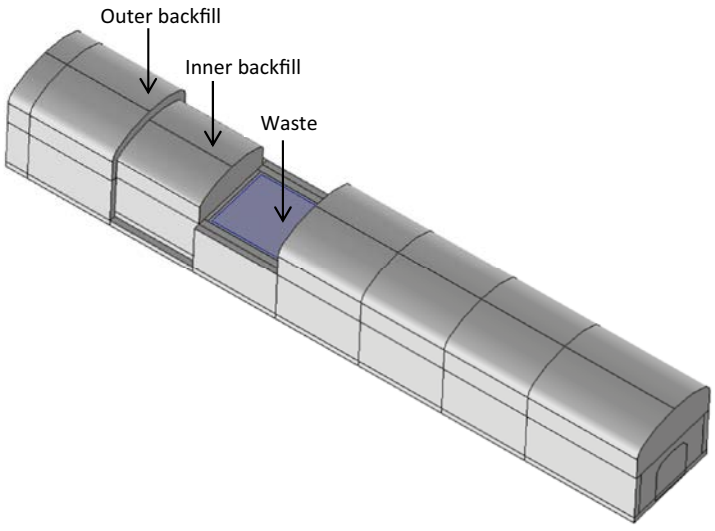


***Figure 3-1.*** *Geometry of the BHK vault showing the different control volumes: outer and inner concrete backfill, and waste domain.*

In particular, at a given time, input to the radionuclide transport model consists of a single representative value of each property for each control volume (inner and outer backfill). The proposed methodology to calculate these values is based on the following assumptions:

- The evolution of concrete backfill on the left side of the waste domain is considered to provide representative parameters for the entire outer and inner backfill with time. This region is the most degraded part of the concrete backfill (see Idiart and Shafei 2019).
- The diffusion coefficient and hydraulic conductivity correspond to equivalent values obtained using a series model, separately over the inner and outer backfill (Equations 3-1 and 3-2).
- Local (i.e. elementwise) values are calculated following equations in the next section (4-1 and 4-2).
- Porosity and pH values are calculated based on the weighted mean at different distances from the backfill outer boundary (Equations 3-3 and 3-4).

Depending on the nature of each variable, either a series model or a model based on the weighted average is used. Equivalent transport properties along the direction of flow are calculated using a series model. On the other hand, mean values of porosity and pH over the control volumes are calculated based on a weighted average.

The equivalent effective diffusion coefficient resulting from the 1D reactive transport simulation is calculated over 1 million years using the following equation:

$$D_e^{eq} = \frac{L}{\int_a^b \frac{1}{D_e(x,t)} dx} \tag{3-1}$$

Above, $D_e(x,t)$ is the local effective diffusion coefficient, $a$ (m) and $b$ (m) correspond to the x coordinate of the boundaries where the integration is calculated and $L$ (m) is the calculated backfill thickness ($b$-$a$). Thus, $L$ is 1.4 m for the control volumes and 2.8 m for the complete backfill.

Analogously, the equivalent hydraulic conductivity resulting from the reactive transport simulation can be calculated as

$$K_h^{eq} = \frac{L}{\int_a^b \frac{1}{K_h(x,t)} dx} \tag{3-2}$$

The porosity is calculated with the following equation:

$$\varphi = \frac{\int_a^b \varphi(x,t) dx}{L} \tag{3-3}$$

In turn, pH is calculated as:

$$pH = \frac{\int_a^b pH(x,t) dx}{L} \tag{3-4}$$

# 4 Description of conceptual model

A cross section of the BHK vault is shown in Figure 4-1. The 1D model considered in this work, is a line cutting the left-hand side of the concrete backfill. The 1D geometry is bounded by the contact with the rock (left) and the waste domains (right).

The parameterisation of the model is exactly the one used for the Base Case (Case I) in Idiart and Shafei (2019). For completeness, the input data is specified below. Initial material properties for flow and transport are presented in Table 4-1. These properties may evolve with time due to mineral dissolution/precipitation processes in the concrete barrier. The coupling between concrete degradation and material properties that has been considered here is based on variations in porosity. Chemical reactions leading to mineral dissolution and precipitation cause the porosity changes. The affected flow and transport parameters are hydraulic conductivity, $K$ (m/s), and effective diffusion coefficient, $D_e$ ($m^2$/s).

The chemical setup is based on the use of the thermodynamic database CEMDATA07 (e.g. Lothenbach et al. 2008). This database has been rewritten in Phreeqc format by Jacques (2009). All chemical reactions have been calculated assuming thermodynamic equilibrium. The initial concrete porewater composition is given in Table 4-2. The porewater composition is in equilibrium with the mineral phases. The mineralogical phase assemblage of concrete and exchanger composition to represent alkali uptake in cement paste are presented in Table 4-3. The chemical composition is based on the work by Höglund (2014). Table 4-4 presents the secondary minerals that are allowed to precipitate in case supersaturation of the solution is reached.

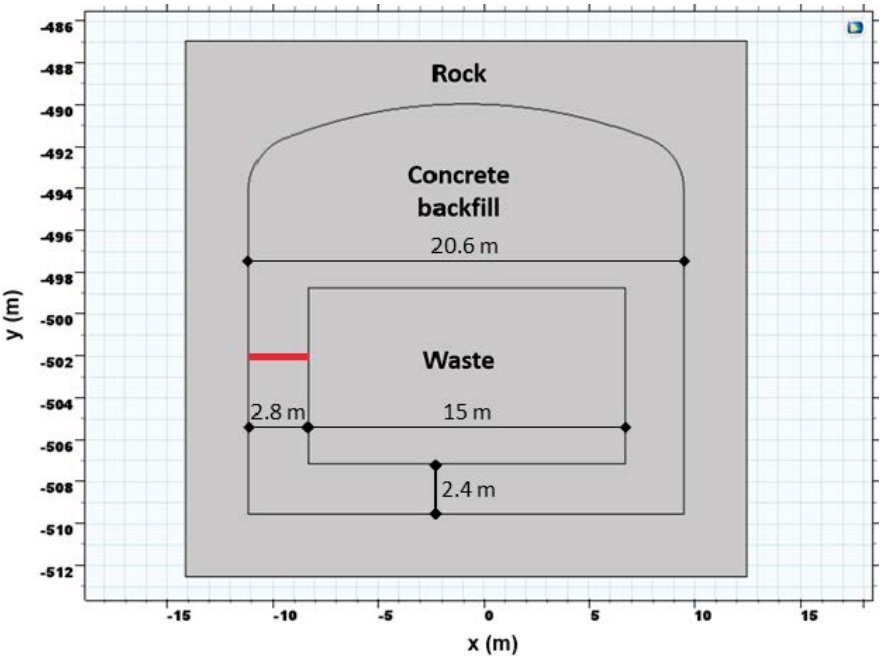


***Figure 4-1.*** *Position of the 1D studied domain (in red) referred to the 2D cross-section of BHK vault, dimension in metres (m), the 1D geometry is fully contained in the concrete backfill domain.*

**Table 4-1. Physical properties of concrete from Idiart and Shafei (2019).**

| Porosity, $\varphi_0$ | Tortuosity, $\tau$ | $D_e$ (m$^2$/s) | $K_0$ (m/s) |
|---|---|---|---|
| 0.11 | 0.0318 | $3.50 \times 10^{-12}$ | $8.30 \times 10^{-10}$ |

**Table 4-2. Granitic groundwater and concrete porewater compositions from Idiart and Shafei (2019).**

| | Groundwater | Concrete porewater |
|---|---|---|
| pH | 8.64 | 12.975 |
| Temperature (°C) | 25 | 25 |
| Ionic strength (M) | 0.007 | 0.128 |
| **Species (totals)** | **Concentration (M)** | |
| Al | 1.21E-06 | 5.542E-07 |
| C | 6.91E-04 | 1.001E-05 |
| Ca | 5.26E-04 | 3.684E-03 |
| Cl | 4.53E-03 | 5.550E-05 |
| K | 7.60E-05 | 8.837E-02 |
| Mg | 1.48E-04 | 2.526E-08 |
| Na | 4.79E-03 | 2.698E-02 |
| S(6) | 3.73E-04 | 3.289E-03 |
| Si | 1.42E-04 | 4.522E-05 |

**Table 4-3. Mineralogical phase assemblage of concrete from Idiart and Shafei (2019). The chemical composition of the minerals and their equilibrium constants are presented in Appendix A.**

| Primary mineral | Concrete<br>Concentration (mol/l$_{medium}$) | Concentration (M) | Volume fraction (-) |
|---|---|---|---|
| Portlandite (CH) | 1.60160 | 14.56 | 0.053 |
| $CSH_{jen}$ | 1.20890 | 10.99 | 0.094 |
| Ettringite | 0.01219 | 0.111 | 0.009 |
| Hydrogarnet Si | 0.10450 | 0.95 | 0.015 |
| Thaumasite | 0.03498 | 0.318 | 0.012 |
| Hydrotalcite OH | 0.01694 | 0.154 | 0.004 |
| Porosity | - | - | 0.110 |
| Inert fraction | - | - | 0.704 |
| Total | - | - | 1.000 |
| **Exchanger composition** | **(mol/l$_{medium}$)** | **(M)** | |
| $CaX_2$ | 0.000374 | 0.0034 | |
| KX | 0.053537 | 0.4867 | |
| NaX | 0.007910 | 0.0719 | |

**Table 4-4. Secondary minerals allowed precipitating. The chemical composition of the minerals and their equilibrium constants are presented in Appendix A.**

| Secondary mineral |
|---|
| $CSH_{tob2}$ |
| Monocarboaluminate |
| Hydrogarnet OH |
| Monosulfoaluminate |
| Calcite |
| Brucite |
| Hemicarboaluminate |
| Gypsum |
| Hydrotalcite C |
| $SiO_2$ am |

Chemical degradation is represented as a sequence of dissolution/precipitation reactions involving mineral phases. This process has a direct consequence on the total porosity. Hydraulic conductivity and the effective diffusion coefficient depend to a large extent on porosity. Therefore, a coupling scheme between physical and chemical processes is needed to correctly capture this feedback. The dependence of hydraulic conductivity on porosity is modelled through the well-known Kozeny-Carman relation (Carman 1937):

$$K(\varphi) = K(\varphi_0)\frac{(1-\varphi_0)^2}{\varphi_0^3}\frac{\varphi^3}{(1-\varphi)^2} \quad (4\text{-}1)$$

In this equation, $K(\varphi)$ is the hydraulic conductivity (m/s), which is a function of porosity ($\varphi$, $m^3/m^3$), and $K(\varphi_0)$ is the hydraulic conductivity (m/s) associated with the initial porosity ($\varphi_0$, $m^3/m^3$). In Appendix C, the effect of considering a different relation between hydraulic conductivity and porosity, namely the modified Kozeny-Carman relation, is assessed.

The effective diffusion coefficient ($m^2/s$) depends on porosity as well, following the equation:

$$D_e = \tau\varphi_0 D_0 \left(\frac{\varphi}{\varphi_0}\right)^n \quad (4\text{-}2)$$

In Equation (4-2), $n$ is an exponent with an assumed value of 2.5 (Idiart and Shafei 2019), $\tau$ (-) is the tortuosity of the porous medium, and $D_0$ ($m^2/s$) is the diffusion coefficient in free water, assumed to be $1.0 \times 10^{-9}$ $m^2/s$.

The boundary conditions for solute transport are fixed concentration at the left boundary and no concentration gradient at the right boundary. The groundwater composition used in the simulation is shown in Table 4-2. For flow, a constant hydraulic head gradient is imposed as to obtain a Darcy flow of $1.03 \times 10^{-11}$ m/s at time zero (Abarca et al. 2016). As degradation proceeds, the hydraulic conductivity gradually increases from left to right, leading to an increased equivalent hydraulic conductivity of the 1D domain. For a constant hydraulic head gradient, this increase translates linearly to higher Darcy velocities.

# 5 Numerical model setup

The conceptual model described in Chapter 4 is implemented in iCP (Nardi et al. 2014), a software interface between Comsol Multiphysics version 5.2 (COMSOL 2015) and Phreeqc version 3 (Parkhurst and Appelo 2013). This section presents the details of the numerical implementation.

A spatial discretization of 0.1 m long finite elements is used (Figure 5-1), giving a total number of 28 elements.

The simulation time of 1 million years is discretized with constant communication time steps between Comsol and Phreeqc set to 10 years. In order to set up the time step size for the given finite element mesh, groundwater flow conditions, and the effective diffusion coefficient (dispersivity is assumed negligible), two criterions have been applied. The first one is the Von Neumann criterion for preventing numerical oscillations, which yields:

$$\Delta t \leq \frac{\Delta x^2}{2D_L} \tag{5-1}$$

where $\Delta t$ (s) is the time step size, $\Delta x$ (m) is the finite element size, and $D_L$ (m$^2$/s) is the dispersion-diffusion tensor.

The second criterion is given by the Courant number ($C_r$). This criterion states that the time step size must be smaller than the time for water to travel to adjacent grid points. If $v$ (m/s) is the component of interstitial velocity, the Courant condition is simply:

$$C_r = \frac{v_i \Delta t}{\Delta x_i} < 1 \qquad \text{or} \qquad \Delta t < \frac{\Delta x_i}{v_i} \tag{5-2}$$

In the same way as for the first criterion, the theoretically maximum time step can be calculated using Equation (5-2) as a function of the mesh refinement and groundwater velocities.

For the given finite element mesh and groundwater flow field, the application of the initial Courant and Von Neumann stability criterions yield the initial maximum time steps shown in Table 5-1.

The Péclet number of the 1D model assuming the entire backfill thickness ($L_b$) is calculated as

$$Pe = \frac{qL_b}{\varphi D_e} \tag{5-3}$$

where $q$ is the Darcy velocity (m/s). The initial Péclet number of the 1D model is ~75, indicating a larger contribution of advection to solute transport, compared to diffusive fluxes. Appendix C presents a more detailed analysis of the processes of solute transport in the model system. It shows that even though advection is the dominant solute transport mechanism, diffusion is a non-negligible process.

As degradation proceeds, the transport properties locally increase from left to right as a result of an increase in porosity. Thus, the equivalent transport properties of the modelled domain also increase with time, as detailed in Chapter 3. These variations impact the Darcy velocity and the Péclet number of the 1D model as calculated with Equation 5-3. Figure 5-2 presents the evolution in time of the equivalent transport properties, average porosity, and Péclet number, relative to their initial values.

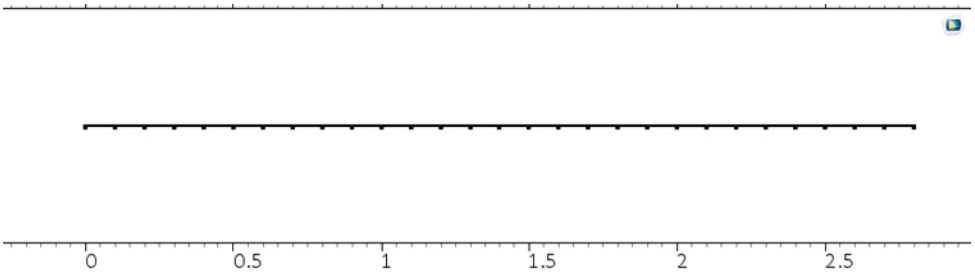


***Figure 5-1.*** *Finite element mesh used in the iCP simulations. Dimension expressed in meters (m).*

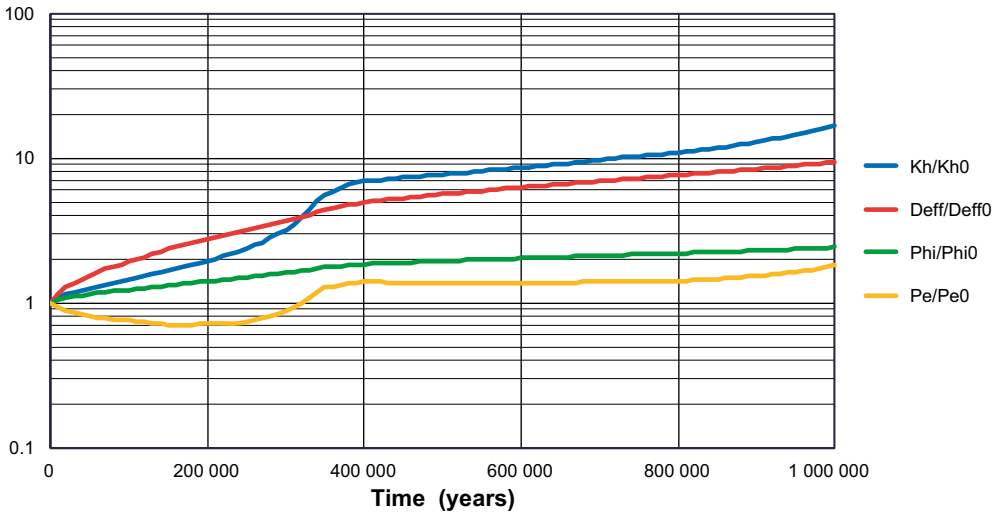


***Figure 5-2.*** *Relative variation of equivalent hydraulic conductivity, equivalent effective diffusivity, average porosity and Péclet number of the full concrete backfill thickness (i.e. 2.8 m) as a function of time; increases referred to initial value of each parameter.*

It may be observed how all the four parameters increase with time. The exception is the Péclet number, which decreases during the first ~200 000 years and then follows a similar increasing tendency as the hydraulic conductivity. After 1 million years, the Péclet number is around twice the initial value, indicating a non-negligible increase of the influence of advective transport over diffusion.

The maximum time step according to the Courant stability criterion decreases with time, although it remains higher than 10 years throughout the simulation time as long as cement hydrates remain in the system. In turn, the maximum time step according to the Von Neumann stability criterion also decreases with time, locally reaching values of down to ~5 years after several hundred thousand years, when hydrates are no more present and advection dominates the degradation. Based on this analysis, time steps of 10 years have been selected for the communication times between the multi-physics (Comsol) and chemical (Phreeqc) solvers.

A detailed analysis of the numerical setup in terms of spatial and temporal discretization is presented in Appendix C.

**Table 5-1. Maximum theoretical initial time-step according to Von Neumann (Equation 5-1) and Courant (Equation 5-2) criterions for the given spatial discretization and material properties.**

| Criterion | Maximum time step (years) |
|---|---|
| Courant | 30 |
| Von Neumann | 45 |

Boundary conditions to simulate groundwater flow are set as a constant hydraulic head gradient of 0.0124 so as to ensure an initial Darcy velocity of $1.03 \times 10^{-11}$ m/s from left to right. This value corresponds to an average flow from the results obtained by Abarca et al. (2016).

As degradation proceeds, the Darcy velocity increases as a result of the increase in hydraulic conductivity. The Darcy velocity is proportional to the equivalent hydraulic conductivity of the modelled domain, as defined by Equation 3-2.

For solute transport, the boundary conditions are fixed concentration on the left boundary and outflow condition on the right. The fixed concentration condition is imposed at the rock-concrete interface, assuming a fast renewal of groundwater. The outflow condition is set at the waste-concrete interface, where the waste domain is represented as an outflow boundary for concentration:

$$\boldsymbol{n} \cdot (-\boldsymbol{D_e} \nabla \boldsymbol{c}) = 0 \qquad (5\text{-}4)$$

where, $\boldsymbol{n}$ (-) is the normal vector and $\boldsymbol{c}$ (M) is the solute concentration vector.

# 6 Results

The results are illustrated either as 1D spatial distributions at given times or time evolution of variables at given points. Moreover, results are also post-processed by spatial integration of key parameters needed in the radionuclide transport model. In this latter case, the total domain is subdivided into two halves, representing the outer and inner concrete backfill.

## 6.1 Reactive transport model

The results of the previously described 1D reactive transport model are presented in Figure 6-1 to Figure 6-6. The evolution of the mineralogical phase assemblage at different points is presented in Figure 6-1 in terms of volume fraction ($m^3$ of mineral/$m^3$ of concrete). The spatial distribution at different times is shown in Figure 6-2. The degradation sequence can be clearly observed. The dissolution of portlandite and ettringite is followed by C-S-H decalcification. Subsequently, the dissolution of other hydrates and precipitation of calcite and hydrotalcite C is observed. It is also observed how different time periods are needed between complete portlandite dissolution and the beginning of C-S-H decalcification depending on the point analysed. This time period first increases as a function of the distance to the inlet. However, at some point between x=1.4 and x=2.1 m this tendency is reversed, and this time period is reduced. The reason is the evolution of the transport properties, as exemplified by the Péclet number in Figure 5-2. After 1 million years of interaction with groundwater, the concrete backfill is almost fully degraded. Partially decalcified C-S-H is the main hydrate near the contact with the waste domain, while calcite formation is significant in the rest of the concrete backfill.

Figure 6-3 presents the evolution of the pH of the pore solution starting from an initial value of 12.97. After full chemical degradation of concrete, a final pH value of ~8.6 is reached, corresponding to the value of groundwater (Table 4-2). After 100 000 years, the inner backfill is virtually unaffected, and only the alkalis have been leached. The pH is governed by portlandite solubility and has a constant value of 12.5. The outer backfill, on the other hand, has undergone significant portlandite dissolution over a thickness of 1 m. Portlandite completely dissolves in the outer backfill after approximately 180 000 years. In the inner backfill this takes around 340 000 years. C-S-H starts decalcifying after portlandite is depleted, although this process is very slow. In the outer backfill, C-S-H completely dissolves only after ~800 000 years.

All these mineralogical alterations are coupled to porosity changes, as shown in Figure 6-4. In turn, porosity changes affect the flow and transport properties of the concrete barrier, see Figure 6-5. As a result of the dissolution process, porosity substantially increases from the initial value of 0.110 to up to 0.296. The concrete mix used in this study contains an aggregate volume fraction of ~0.70 $m^3$ of aggregates/$m^3$ of concrete. Therefore, a porosity of 0.296 in the concrete backfill corresponds to a situation where all the hardened cement paste is completely degraded. These porosity values do not account for the clogging effects of carbonation (i.e. calcite precipitation), which may be regarded as a conservative assumption. After 1 million years, almost the entire concrete backfill has a porosity equal to full dissolution of the cement hydrates.

The evolution of hydraulic conductivity and effective diffusion coefficient is analysed in Figure 6-5, where its porosity dependence is clearly shown. Initial values for hydraulic conductivity and effective diffusion coefficient are $8.3 \times 10^{-10}$ m/s and $3.5 \times 10^{-12}$ $m^2$/s, respectively. The highest values, found at the rock-concrete interface, are $2.5 \times 10^{-8}$ m/s and $4.1 \times 10^{-11}$ $m^2$/s, respectively. These changes lead to a gradual increase of the relative impact of advective over diffusive transport, as indicated by the evolution of the Péclet number of the concrete backfill (Figure 5-2). For a constant hydraulic head gradient, the increase in Darcy velocity is directly proportional to the increase in the equivalent hydraulic conductivity calculated with Equation 3-2. This Darcy velocity is shown in Figure 6-6.

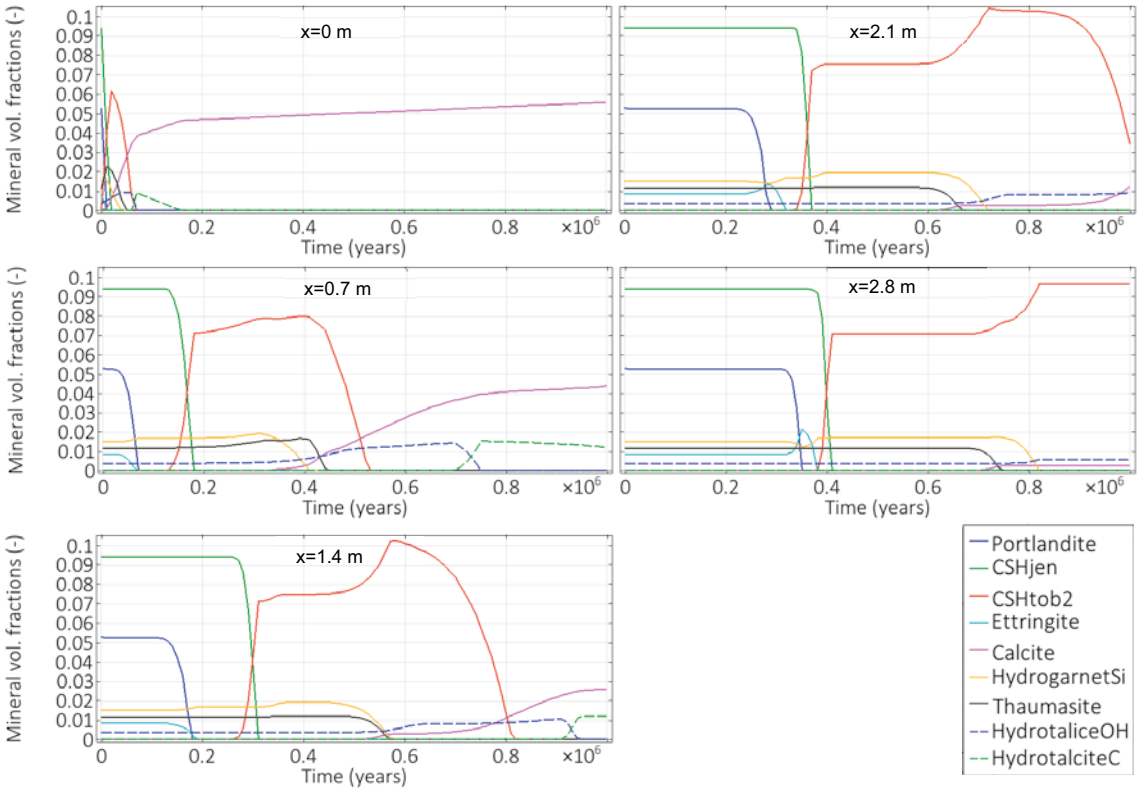


***Figure 6-1.*** *Mineral volume fractions as a function of time (years) at different points of the concrete backfill: buffer-rock interface (x=0 m); outer backfill mid-point (x=0.7 m); interface between inner and outer backfill (x=1.4 m); inner backfill mid-point (x=2.1 m); concrete backfill-waste interface (x=2.8 m).*

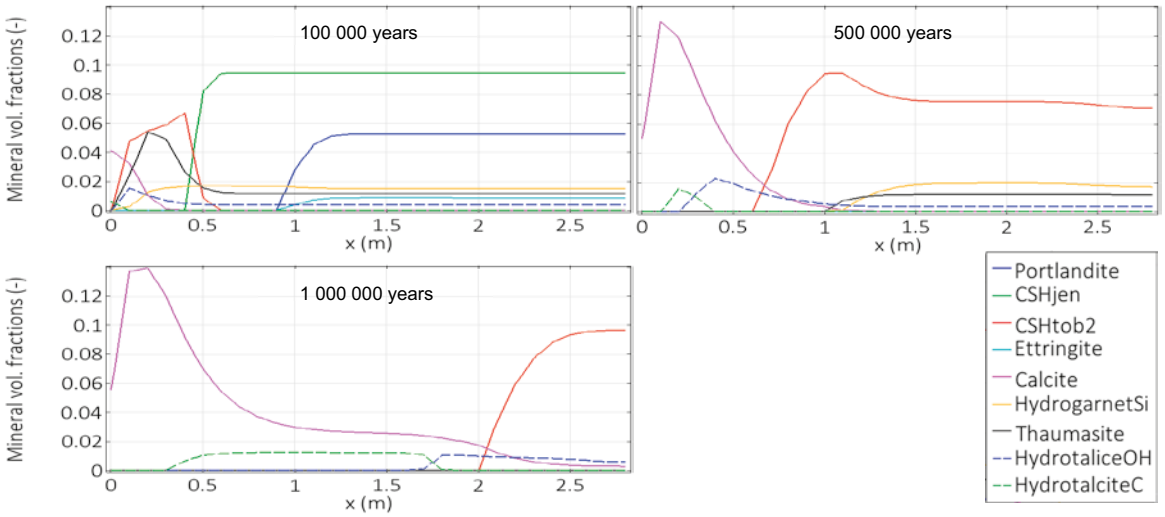


***Figure 6-2.*** *Mineral volume fractions at different times, spatial distribution in the concrete backfill (length in m).*

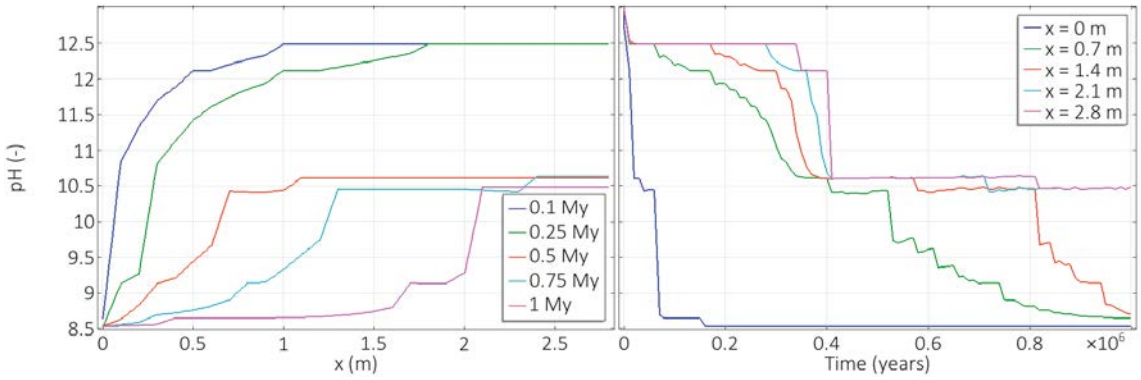


***Figure 6-3.*** *pH (-) spatial distribution at different times (left) and as a function of time at different points of the concrete backfill (right).*

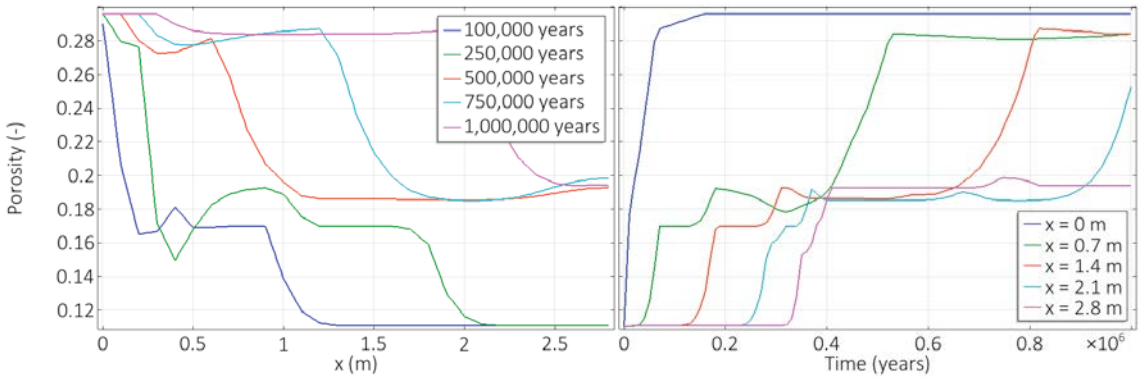


***Figure 6-4.*** *Porosity (-) spatial distribution at different times (left) and as a function of time at different points of the concrete backfill (right).*

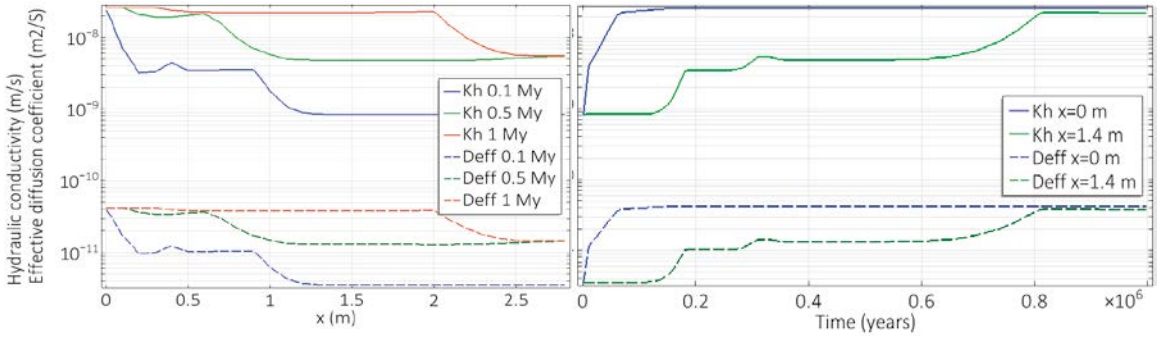


***Figure 6-5.*** *Hydraulic conductivity (m/s) and effective diffusion coefficient ($m^2$/s) spatial distribution at different times (left) and as a function of time (years) at the left boundary and central point of the concrete backfill (right).*

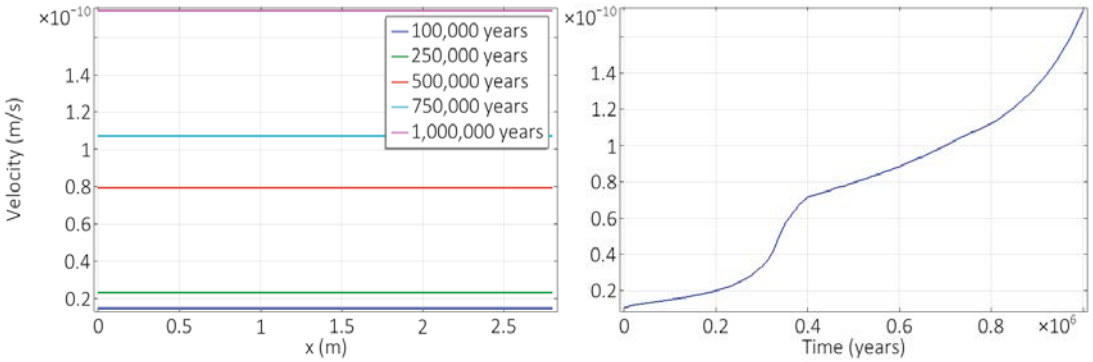


***Figure 6-6.*** *Darcy velocity (m/s) spatial distribution at different times (left) and as a function of time (right).*

## 6.2 Evolution of key parameters

The evolution of pH, porosity, effective diffusivity, and hydraulic conductivity of concrete in the outer and inner backfill are given Figure 6-7 through Figure 6-10. Results corresponding to the two control volumes are post-processed from the reactive transport simulation (Section 6.1) according to the formulation presented in Chapter 3. pH values are also analyzed locally, as shown in Table B-1 of Appendix B for the control volume boundaries (between the inner and outer backfill, and between the outer backfill and waste domain).

As expected, the results indicate that the inner backfill has a substantially slower degradation rate compared to the outer backfill. For example, porosity starts to deviate from its initial values only after ~10 000 years. pH decreases from the initial value of 13 to 12.5 after a relatively fast leaching of Na and K alkalis (less than 10 000 years). After 1 million years, pH in the outer backfill is very close to the groundwater value of ~8.6. In the inner backfill the presence of partly decalcified C-S-H controls the pH to a value of ~9.8.

Concrete degradation is driven by dissolution of cement hydrates, increasing porosity. This is clearly shown in Figure 6-8. The times at which the rate of porosity changes correspond to the times where portlandite and C-S-H gels have completely leached in a control volume. These leaching events are tabulated in Table B-2 (Appendix B), where key porosity and effective diffusion coefficient values are also presented.

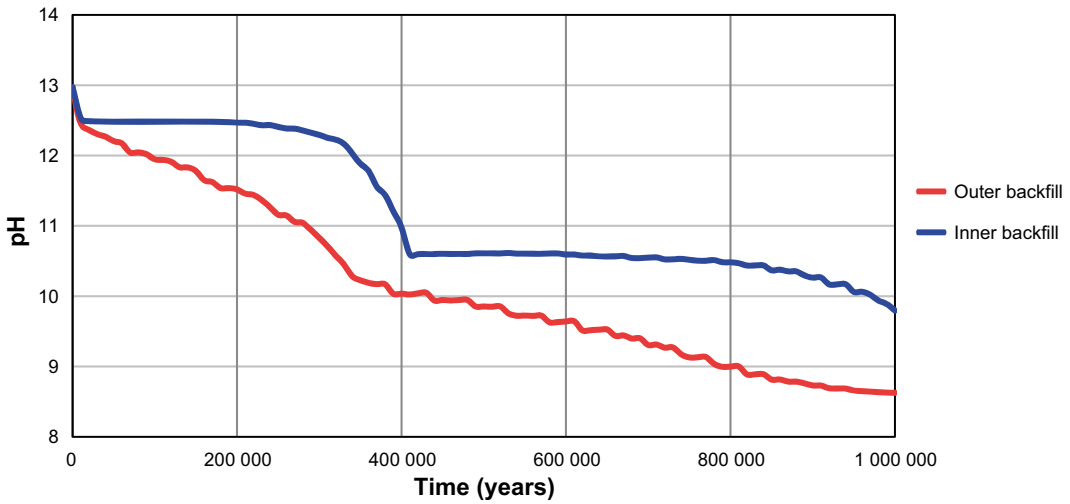


***Figure 6-7.*** *pH (-) value of pore water as a function of time (years), representative values for the inner and outer backfills.*

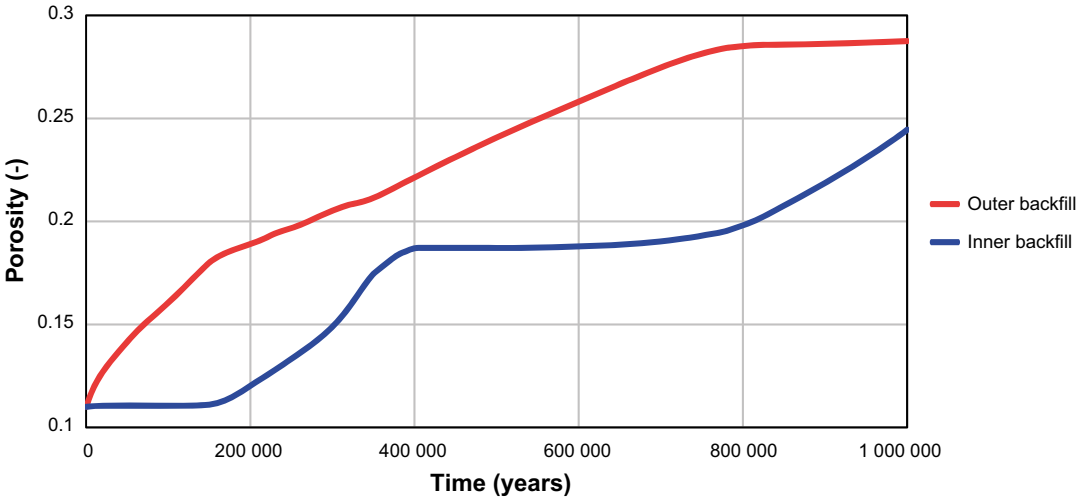


***Figure 6-8.*** *Porosity (-) values as a function of time (years), representative values for the inner and outer backfills.*

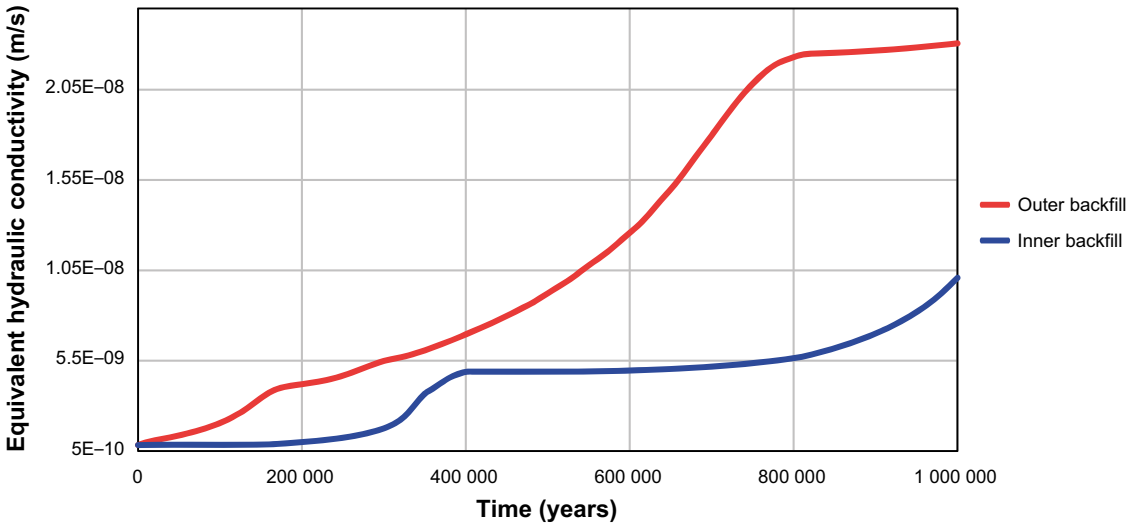


***Figure 6-9.*** *Equivalent hydraulic conductivity (m/s) as a function of time (years), representative values for the inner and outer backfills.*

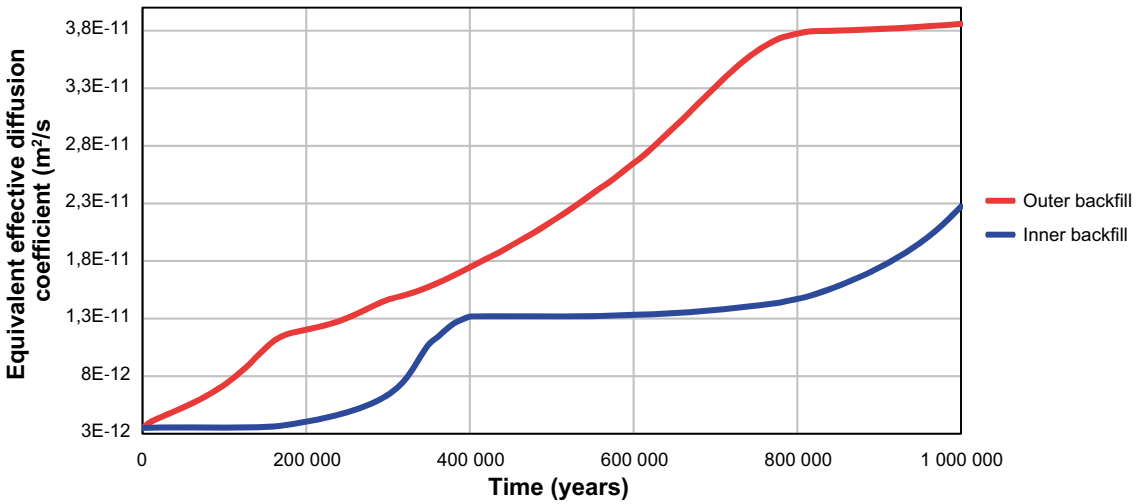


***Figure 6-10.*** *Equivalent effective diffusion coefficient ($m^2/s$) as a function of time (years), representative values for the inner and outer backfills.*

# 7 Comparison with a 2D reactive transport model and analytical solutions

In this section, 1D model results are compared with those obtained by two different models. The first group of results comes from a 2D reactive transport model, defined as the Base Case (Case I) in Idiart and Shafei (2019). This is presented in Section 7.1. In addition, in Section 7.2 results are compared with analytical solutions calculated using the shrinking core model (Levenspiel 1972).

## 7.1 2D reactive transport model results

For comparison, results from the Base Case 2D simulation (Case I in Idiart and Shafei 2019) for the first 100 000 years are presented here. One-dimensional profiles of the concrete backfill at the left of the waste domain are extracted from the 2D results. The reason to restrict the analysis to such profile is that the concrete backfill will be preferentially degraded in this zone. Similar post-processing as for the 1D simulation is performed. The model is defined in detail in Idiart and Shafei (2019) and is similar to the 1D model presented in this report.

Although groundwater flow is similar in both models in terms of initial Darcy velocities, different boundary conditions were used in the 2D simulation. Case I considered an inlet boundary condition on the left border of the rock domain, corresponding to a normal inflow velocity equal to $1.03 \times 10^{-11}$ m/s. On the other hand, a constant hydraulic head gradient is imposed in the 1D model (Chapter 4). In both cases, a similar Darcy velocity is obtained at time zero in the concrete backfill.

The geometry representing the concrete backfill is comparable in both models, but spatial discretization differs. In the 2D model, triangular elements of size ~0.6 m were used, while the 1D model considers 1D elements of 0.1 m width (Section 5-1). This difference in space discretization translates into a different amount of data points for plotting the results. This is clearly shown in Figure 7-1 through Figure 7-5, presenting the spatial distribution of different parameters after 100 000 years. The main difference between the two simulations is the porosity and transport properties near the water inlet. This is due to the fact that in the 1D setup it was decided to calculate porosity without the potentially beneficial effect of carbonation (i.e. calcite precipitation). However, the impact of this assumption is shown to be limited.

From these figures, it may be observed that despite a different discretization, the data points corresponding to the results of the 2D simulation are similar to the results of the 1D model (Figure 7-1). However, in the coarser 2D results there is of course no information about the concrete composition in between data points.

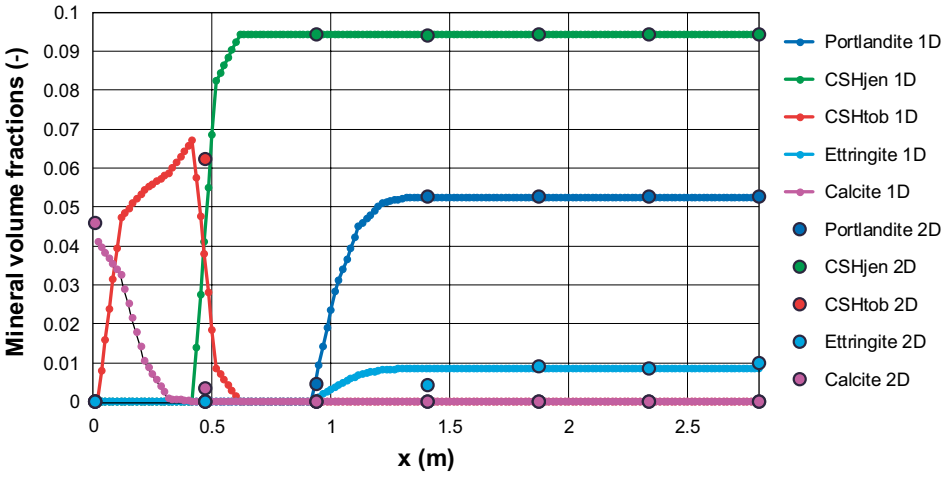


***Figure 7-1.*** *Spatial distribution in the concrete backfill thickness of mineral volume fractions after 100 000 years. Comparison between 1D (solid lines with dots) and 2D (isolated markers) models. Each marker of the 2D model corresponds to a data point. Notice the different spatial discretization used in the two simulations.*

Post-processing of these results to obtain the integrated key parameters for radionuclide transport modelling (Chapter 3) depends on spatial discretization. Spatial integration of the results in Figure 7-2 to Figure 7-5 consists of calculating the area below the curves. Obviously, this area depends on the resolution of the curve, i.e. more data points lead to a more precise integration.

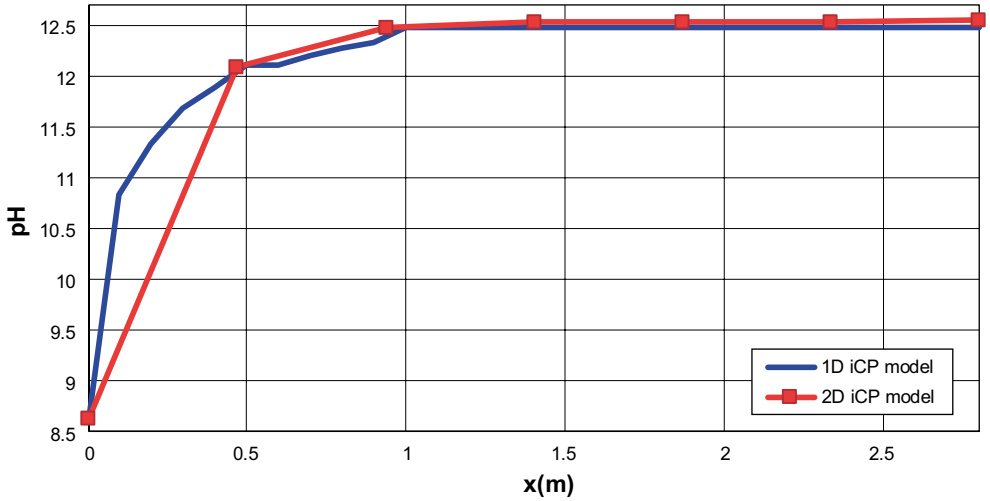


***Figure 7-2.*** *Spatial distribution of pH (-) in the concrete backfill thickness after 100 000 years. Comparison between 1D and 2D models. Each marker corresponds to a data point.*

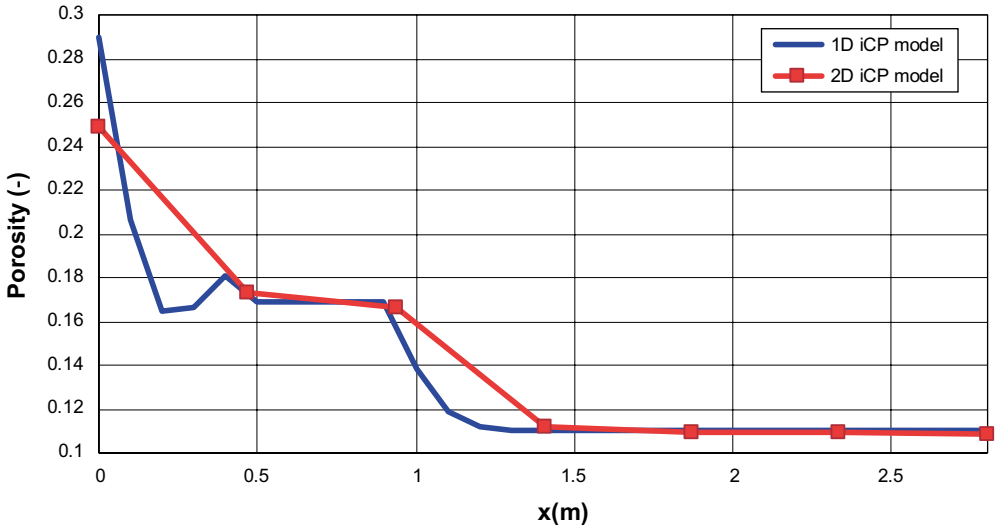


***Figure 7-3.*** *Spatial distribution of porosity (-) in the concrete backfill thickness after 100 000 years. Comparison between 1D and 2D models. Each marker corresponds to a data point.*

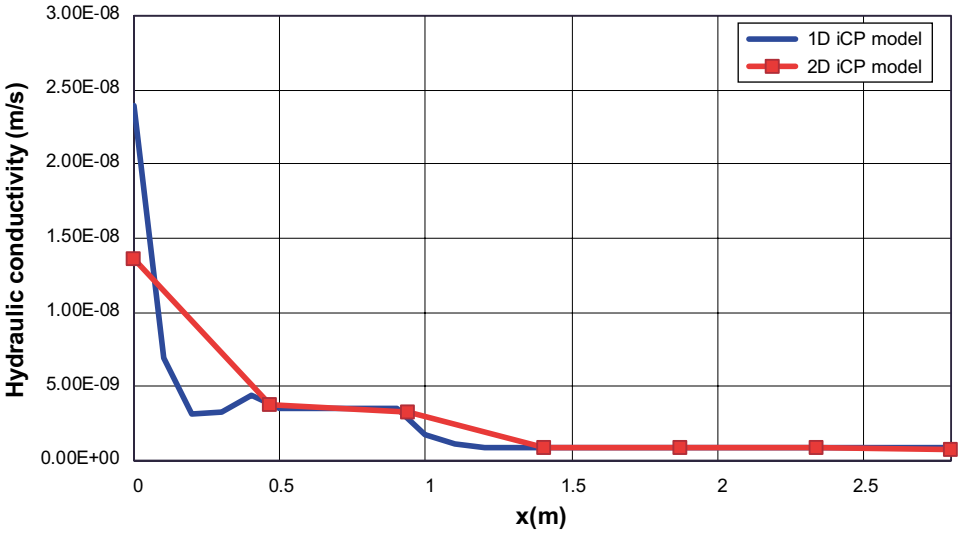


***Figure 7-4.*** *Spatial distribution of hydraulic conductivity (m/s) in the concrete backfill thickness after 100 000 years. Comparison between 1D and 2D models. Each marker corresponds to a data point.*

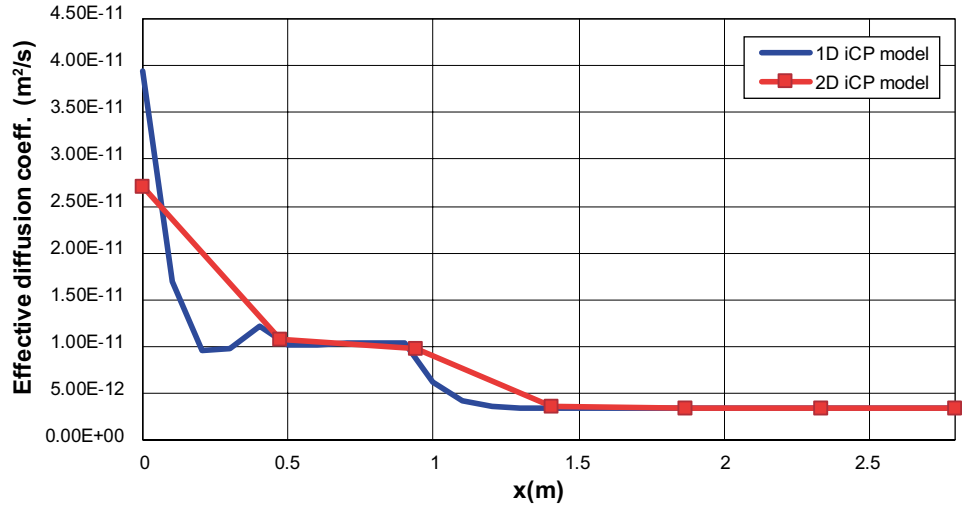


***Figure 7-5.*** *Spatial distribution of effective diffusion coefficient ($m^2/s$) in the concrete backfill thickness after 100 000 years. Comparison between 1D and 2D models. Each marker corresponds to a data point.*

The comparison of results of the post-processing between the 1D and 2D models is presented in Figure 7-6 to Figure 7-9 for pH, porosity, hydraulic conductivity, and effective diffusivity. As in the previous section, key parameters are analysed as single values for the inner and outer backfills. This comparison shows a relatively slower degradation in the 1D model as compared to the 2D Case I. As explained above, this is mainly due to the effect of different spatial discretization on the integration of the key parameters over the thickness of the outer and inner backfill.

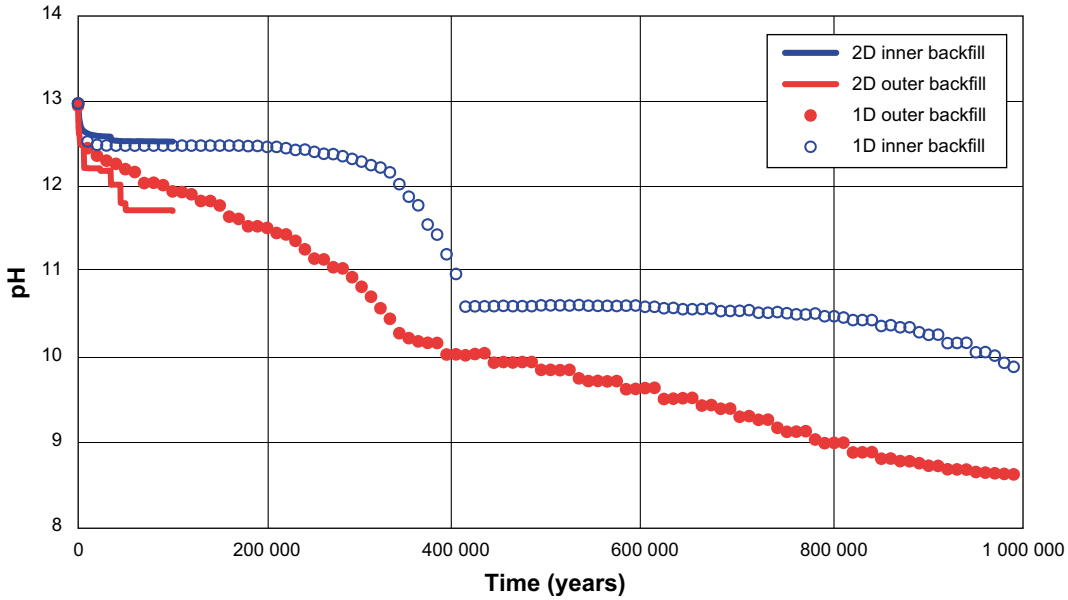


***Figure 7-6.*** *Effective pH (-) as a function of time (years): comparison of representative values for the inner and outer backfill in 1D and 2D models.*

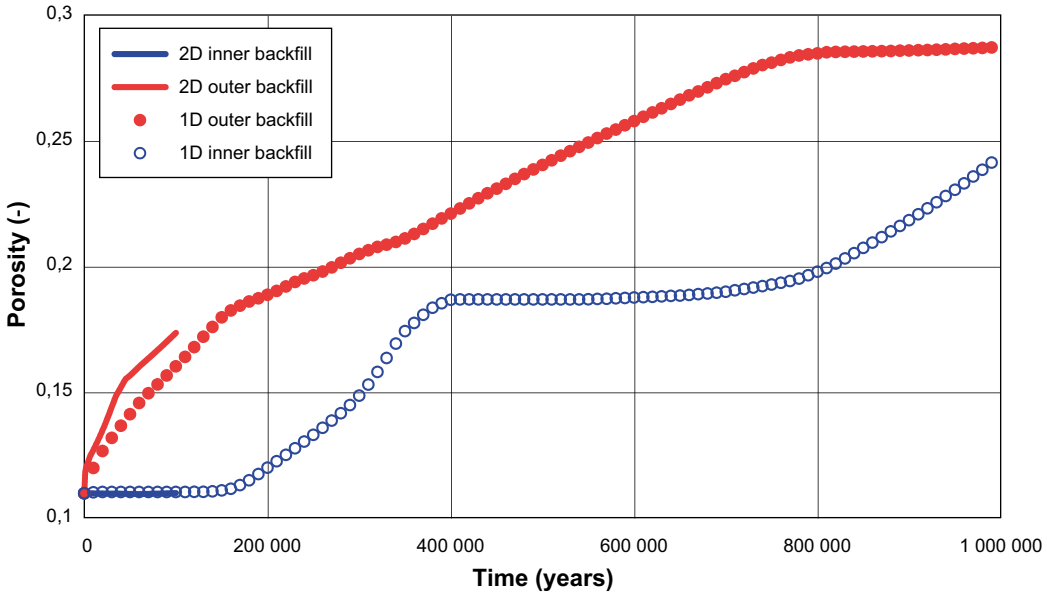


***Figure 7-7.*** *Effective porosity (-) as a function of time (years): comparison of representative values for the inner and outer backfills in 1D and 2D models.*

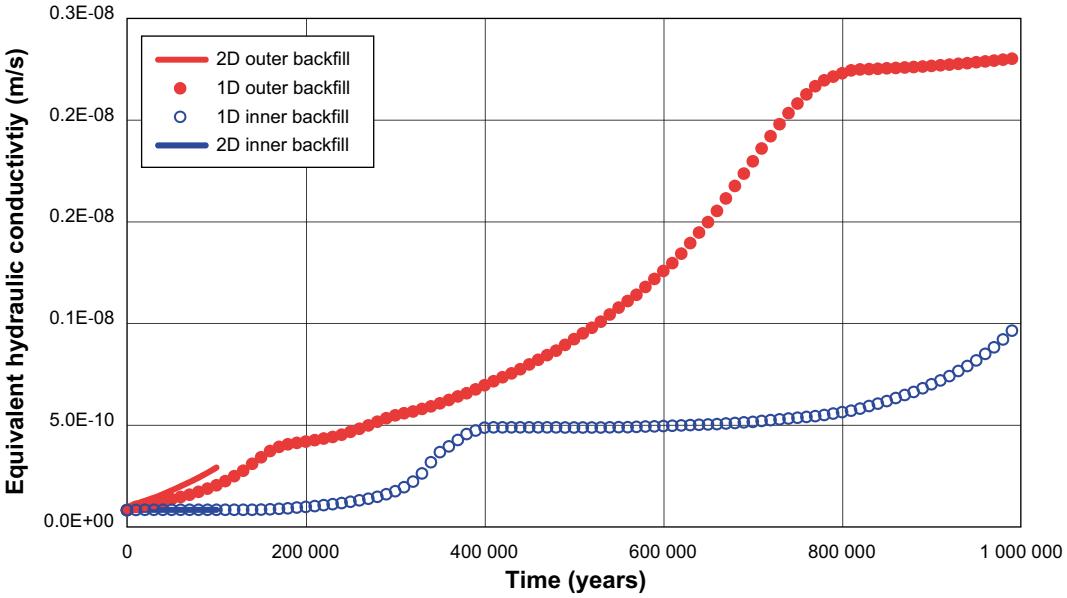


***Figure 7-8.*** *Equivalent hydraulic conductivity (m/s) as a function of time (years): comparison of representative values for the outer backfill in 1D and 2D models.*

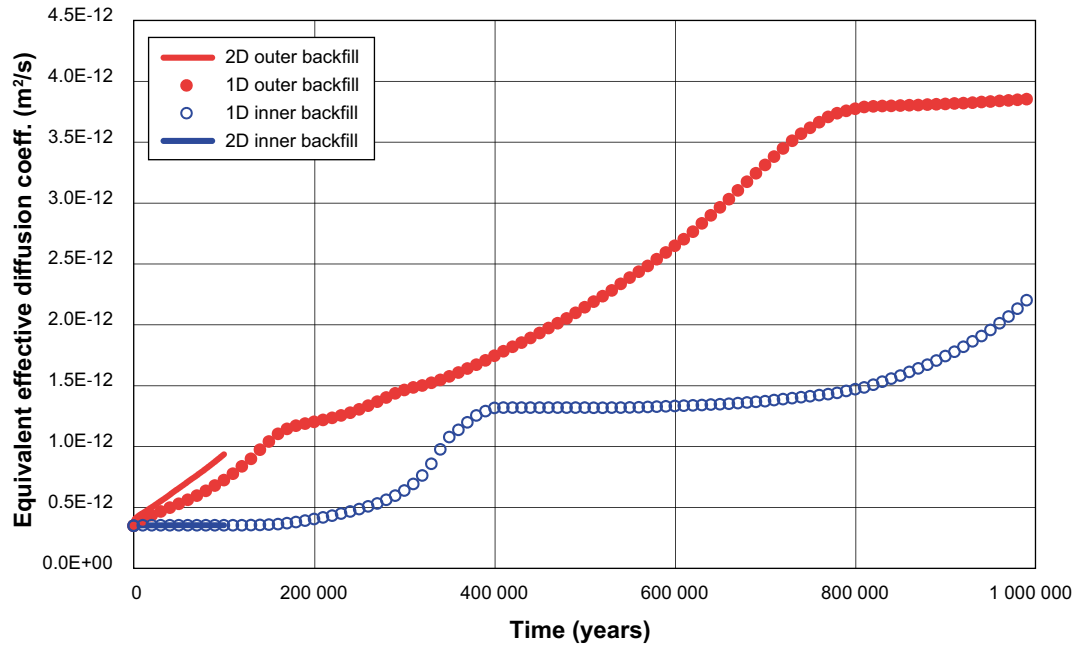


***Figure 7-9.*** *Equivalent effective diffusion coefficient ($m^2/s$) as a function of time (years), comparison of representative values for the outer backfill in 1D and 2D models.*

Another important distinctive feature of the 2D model is the two-dimensional character of Darcy velocity. In a 1D setup all flow is forced in a single direction, while in the 2D model heterogeneities can lead to a non-uniform distribution of the velocity field. In particular, degradation of the concrete backfill near the interface with the rock leads to an increase in the vertical component of the velocity vector. In Figure 7-10, the mid-section of the left concrete backfill is analyzed. Initially, vertical components of the velocity are negligible and the horizontal component is equal to $1.03 \times 10^{-11}$ m/s. However, after 100 000 years, vertical values are significant next to the concrete-rock boundary, while the horizontal velocity profile is relatively unaffected (± 10%).

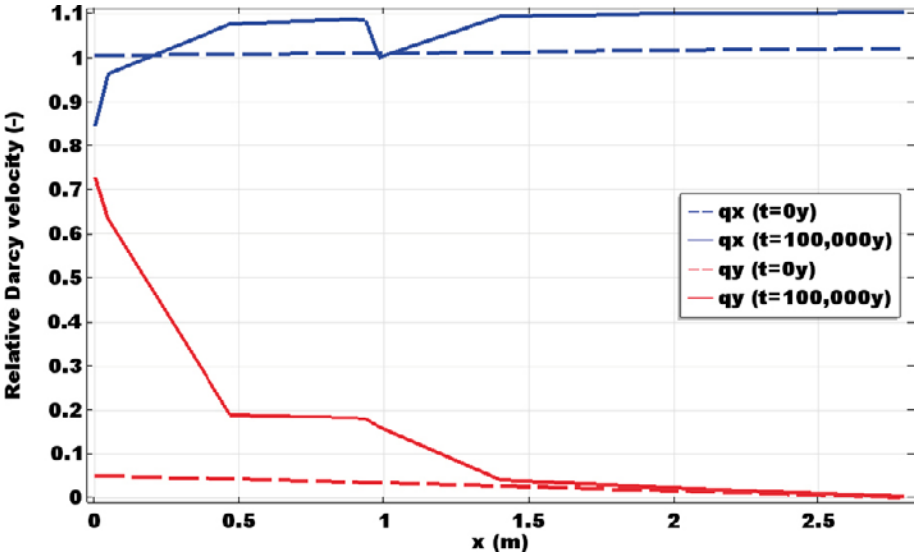


***Figure 7-10.*** *Results from Base Case (Case I) 2D reactive transport model: distribution of Darcy velocities at time zero and after 100 000 years in a one-dimensional profile mid-height of left concrete backfill). Vertical and horizontal component of the Darcy velocity (values referred to the initial value of 1.03 × 10$^{-11}$ m/s).*

On the other hand, the effective diffusion coefficient near the interface with the rock increases up to almost one order of magnitude (Figure 7-5). In the same way, porosity increases (Figure 7-3), resulting in lower pore velocities. As a result, the contribution of advection to solute transport decreases with respect to diffusive transport.

## 7.2 Analytical and semi-analytical solutions

Here, analytical and semi-analytical solutions are used to calculate the evolution of the portlandite and C-S-H leaching depths and their impact on the transport properties. Similar to Höglund (2014), the shrinking core model (SCM) with parameters corresponding to a concrete slab is used (Levenspiel 1972). This model considers diffusion-driven transport and dissolution of a mineral phase under thermodynamic equilibrium conditions. The dissolution depth is expressed as:

$$h_{CH} = \sqrt{2\frac{D_{eff,deg}\cdot Ca_{sol}^{CH}\cdot t}{q_0^{CH}}} \quad (7\text{-}1)$$

or

$$h_{CH-CSH} = \sqrt{2\frac{D_{eff,deg}\cdot (Ca_{sol}^{CH}-Ca_{sol}^{CSH})\cdot t}{q_0^{CH}}} \quad (7\text{-}2)$$

where $h_{CH}$ and $h_{CH\text{-}CSH}$ (m) is the depth of complete portlandite dissolution for a case with only portlandite and a case with C-S-H phases and portlandite, respectively. In the equations above, $D_{eff,deg}$ (m$^2$/s) is a representative value of the effective diffusion coefficient of the degraded region (see below). $Ca^{CH}{}_{sol}$ and $Ca^{CSH}{}_{sol}$ are the solubilities of portlandite and C-S-H, 0.02 and 0.002 mol/liter$_{water}$, respectively, and $q_0{}^{CH}$ (1.6016 mol/liter$_{medium}$) is the initial concentration of portlandite in concrete. The average value of the degraded region, $D_{eff,deg}$, obtained from Figure 7-5 is approximately 1.58 × 10$^{-11}$ m$^2$/s. It follows from Equations (7-1) and (7-2) that the dissolution depth is linearly dependent on the square root of time, which is a characteristic feature of diffusion-driven processes.

Figure 7-11 shows schematically the evolution in time of the portlandite dissolution front, with characteristic parameters $L_{degraded}\ (t)$ (m) and $D_{eff,deg}$ ($m^2/s$). As the dissolution front advances, the horizontal equivalent effective diffusion coefficient of the concrete backfill increases due to the contribution of the degraded region. This can be calculated for the outer and the inner backfill using a series model of a degraded and an intact domain with the following equation:

$$D_{eff}^{equiv} = \frac{L_{backfill}}{\frac{L_{degraded}(t)}{D_{eff,deg}} + \frac{L_{intact}(t)}{D_{eff,0}}} \tag{7-3}$$

An analogous approach can be followed for estimating the equivalent hydraulic conductivity (m/s) for the outer and the inner backfill:

$$K_h^{equiv} = \frac{L_{backfill}}{\frac{L_{degraded}(t)}{K_{h,deg}} + \frac{L_{intact}(t)}{K_{h,0}}} \tag{7-4}$$

The averaged $K_{h,deg}$ value of the degraded region obtained from Figure 7-4 is approximately $5.0 \times 10^{-9}$ m/s.

Figure 7-12 presents the evolution of the portlandite dissolution front as a function of the square root of time resulting from the SCM model and the 1D and 2D reactive transport simulations. By definition, the SCM results show a linear relation between degradation depth and the square root of time. The 2D results also present an almost linear relation, indicating that degradation is mainly governed by diffusion in this case (see discussion in Section 7.1). It may be observed that the SCM approximately matches the reactive transport model results if corrected by the time lag needed to completely dissolve portlandite at the interface between concrete and groundwater. This time lag originates from the fact that in the SCM portlandite dissolution depth starts from time 0, i.e. $h$ (m) > 0 for $t > 0$, according to Equation 7-1. However, in the reactive transport model it takes time to dissolve all the portlandite in the outer concrete layer. The time lag is therefore equal to the time that portlandite takes to fully dissolve in the first node in the reactive transport model.

According to the results of the SCM with only portlandite, it would take ~ 195 000 years and ~ 700 000 years to completely dissolve portlandite along the outer (1.4 m) and inner backfill thickness (2.8 m), respectively (Figure 7-12).

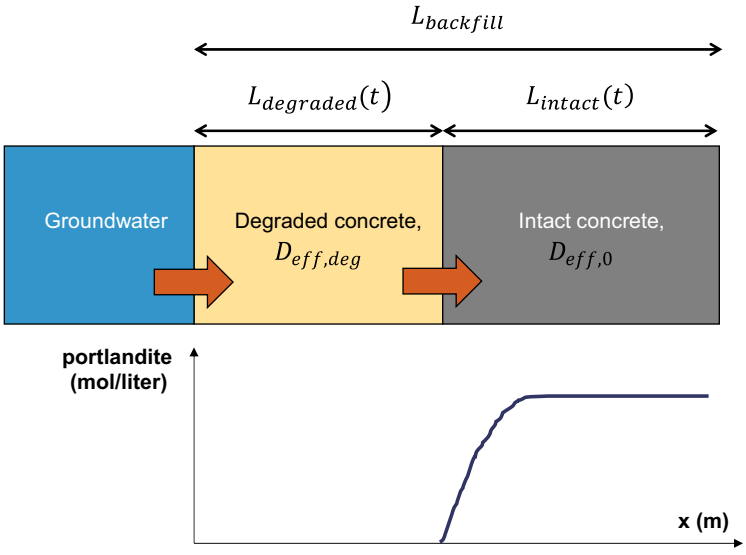


***Figure 7-11.*** *Schematic representation of the degradation of concrete as indicated by the portlandite dissolution front.* $L_{backfill}$ *is 2.8 m for the concrete backfill.*

The 1D reactive transport model results show a non-linear relation between dissolution depth and square root of time (Figure 7-12) or time (Figure 7-13). However, in this case the evolution of the portlandite dissolution depth is clearly advective dominated, characterized by an almost linear relation between depth and time. The reason is mainly due to the monotonous increase in Darcy velocity (Figure 6-6) along the backfill thickness as a function of time. Pure advective systems are characterized by a linear relation between dissolution depth and time. Deviations from linearity are due to the contribution of diffusion, which is not negligible in the present setup (Appendix C).

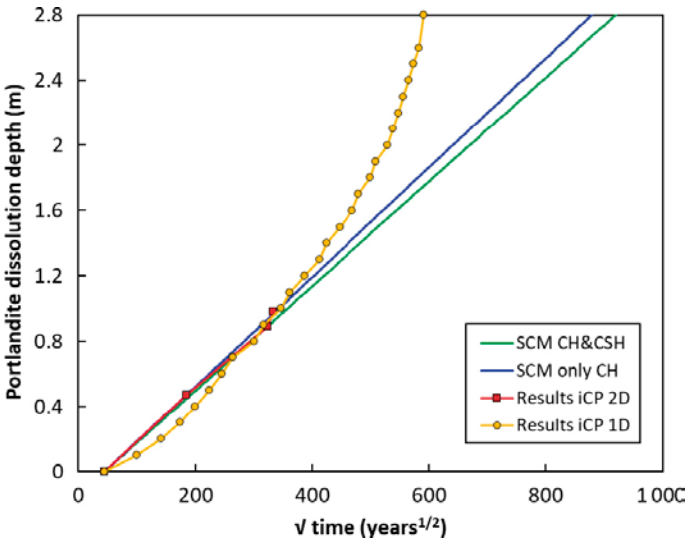


***Figure 7-12.*** *Portlandite dissolution depth (m) in the concrete backfill as a function of square root of time (years$^{1/2}$): results corresponding to iCP and SCM analytical models. Results corrected by the time lag needed to completely dissolve portlandite at the interface between concrete and groundwater.*

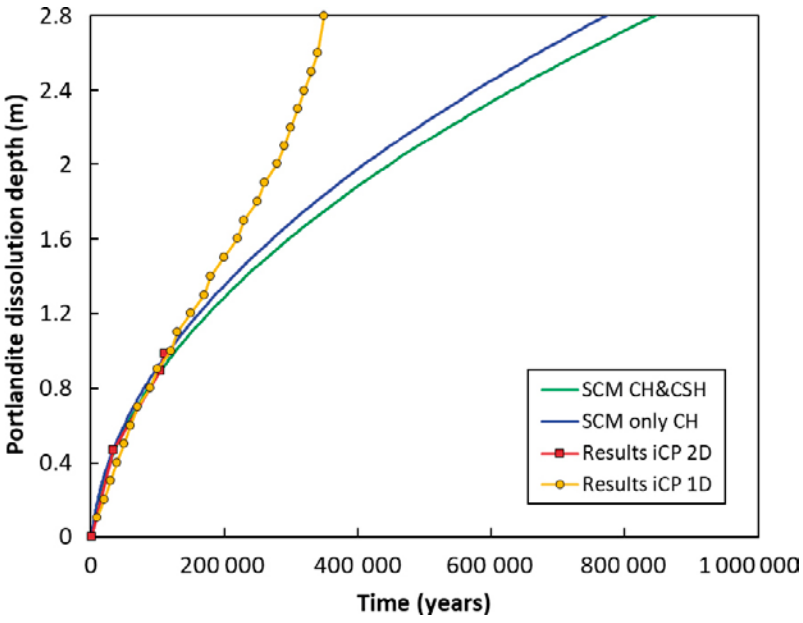


***Figure 7-13.*** *Portlandite dissolution depth (m) in the concrete backfill as a function of time (years): results corresponding to iCP and SCM analytical model.*

Figure 7-14 and Figure 7-15 show the evolution of the equivalent effective diffusion coefficient and hydraulic conductivity resulting from the 1D and 2D reactive transport simulations and the SCM. During the first 100 000 years, the evolution of the equivalent transport properties predicted by the SCM are closer to the 2D reactive transport results than to the 1D simulation. This is due to the similar evolution of the portlandite dissolution depth between the SCM and the 2D model. On the contrary, the 1D reactive transport model shows a much faster increase of transport property values due to the relatively larger influence of advective transport.

The equivalent effective diffusion coefficient of the concrete backfill from the SCM (Figure 7-14) is calculated with Equation (7-3). In this plot, $L_{degraded}\ (t)=h_{CH}$ corresponds to the SCM Equation (7-1). In the same way, the equivalent hydraulic conductivity (Figure 7-15) is calculated with Equation (7-4). The SCM is also used to estimate the evolution of the equivalent transport properties beyond 100 000 years, until portlandite is completely depleted.

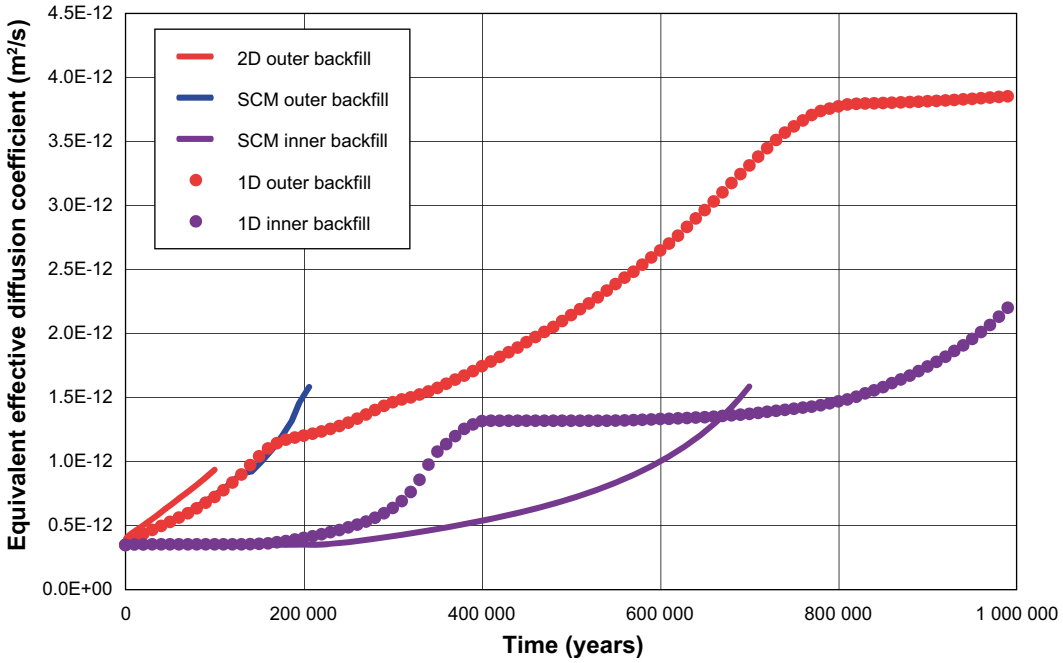


***Figure 7-14.*** *Evolution of the equivalent effective diffusion coefficient ($m^2/s$) of the outer and inner concrete backfill until 1 000 000 years. Results from the shrinking core model (SCM) with only portlandite (CH) until portlandite is completely depleted. Results from iCP models (100 000 years for 2D and 1million years for 1D) are also included.*

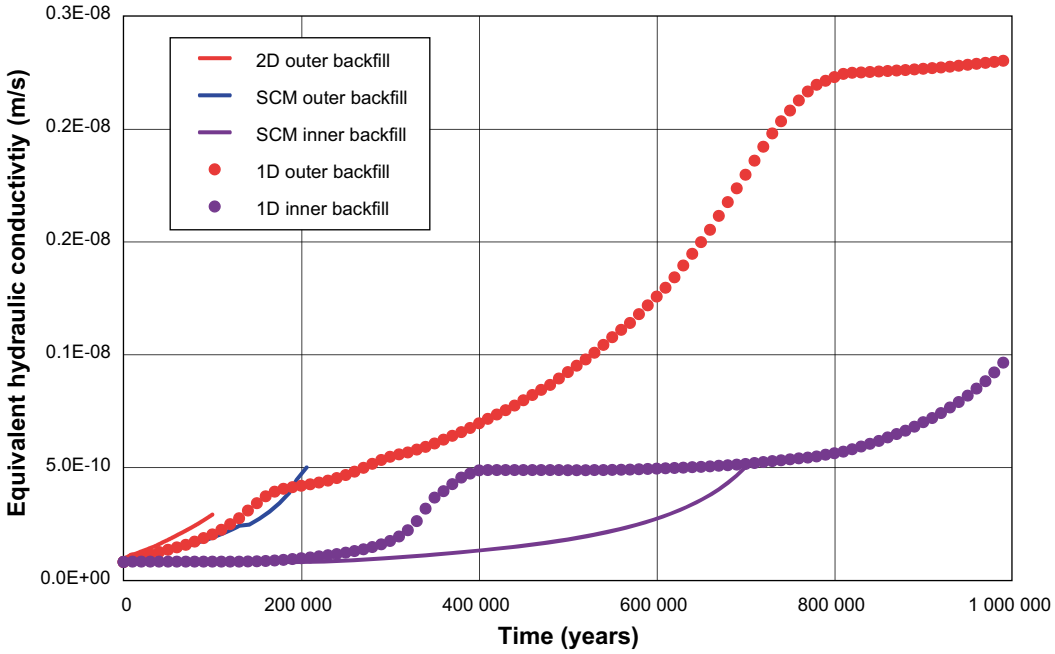


***Figure 7-15.*** *Evolution of the equivalent hydraulic conductivity (m/s) of the outer and inner concrete backfill until 1 000 000 years. Results from the shrinking core model (SCM) with only portlandite (CH) until portlandite is completely depleted. Results from iCP models are also included.*

# 8 Summary and conclusions

A 1D reactive transport model has been used for simulations of concrete degradation in BHK, a rock vault in the proposed repository concept for long-lived low and intermediate level waste (SFL). A software interface between Comsol Multiphysics and Phreeqc (iCP) has been used in the modelling. The focus has been on evaluating the pH, porosity, effective diffusivity and hydraulic conductivity of the BHK concrete backfill over 1-million-year time span.

The main concrete degradation process is driven by leaching of calcium, which leads to gradual dissolution of the main cement hydrates. Calcite precipitation as a result of the carbonate ingress from groundwater and calcium from hydrates dissolution is another important process. After 1 million years, the full thickness of the concrete backfill (2.8 m) is near complete degradation, with calcite precipitating in most of the thickness. Partially degraded C-S-H is only present in the last 80 cm near the waste.

The results obtained with the present 1D model are compared to the Base Case (Case I) 2D reactive transport simulation presented in Idiart and Shafei (2019). However, this comparison is limited to the first 100 000 years, which is the simulation time considered by Idiart and Shafei (2019). The comparison is shown to be satisfactory in terms of spatial profiles of the main chemical indicators. However, the higher spatial resolution of the 1D model allows for a more accurate post-processing of these results to calculate the equivalent transport properties and effective porosity and pH of the concrete backfill.

As expected, the comparison of the post-processed key parameters of the concrete backfill between 1D and 2D reactive transport models shows an only fair agreement. This is mainly due to the effect of spatial resolution on integration of the key parameters over the backfill thickness.

An analytical model based on the shrinking core model (Levenspiel 1972) has also been used to study portlandite and C-S-H dissolution depth, assuming solute transport as a purely diffusive process. The results of the SCM have been compared with the 1D and 2D reactive transport models in terms of the evolution of portlandite dissolution depth and equivalent transport properties.

In the 1D reactive transport model, the constant increase in Darcy velocity with time leads to an advective-dominated degradation process. This is in part due to the assumed boundary condition, which is based on a constant hydraulic head gradient. As a result, fluid flow increases monotonously with time. The comparison with the SCM results is thus poor. In contrast, the 2D reactive transport model shows a more diffusive-dominated degradation process over the first 100 000 years. In this case, the comparison with the SCM shows therefore a relatively good agreement. In that case, the horizontal Darcy velocity is only marginally affected, while porosity and diffusion coefficient increase substantially. The effect of concrete degradation is an increase in the vertical component of the velocity of the degraded region.

# References

SKB's (Svensk Kärnbränslehantering AB) publications can be found at www.skb.com/publications.


**Abarca E, Sampietro D, Miret M, von Schenck H, 2016.** Initial modelling of the near-field hydrogeology. Exploring the influence of host rock characteristics and barrier properties. Report for the safety evaluation SE-SFL. SKB R-16-02, Svensk Kärnbränslehantering AB.

**Abarca E, Sampietro D, Molinero J, von Schenck H, 2019.** Modelling of the near-field hydrogeology – temperate climate conditions. Report for the safety evaluation SE-SFL. SKB R-19-03, Svensk Kärnbränslehantering AB.

**Carman P C, 1937.** Fluid flow through a granular bed. Transactions of the Institution of Chemical Engineers 15, 150–167.

**COMSOL, 2015.** COMSOL Multiphysics, version 5.2. Burlington, MA: COMSOL Inc.

**Elfwing M, Evins L Z, Gontier M, Grahm P, Mårtensson P, Tunbrant S, 2013.** SFL concept study. Main report. SKB TR-13-14, Svensk Kärnbränslehantering AB.

**Höglund L O, 2014.** The impact of concrete degradation on the BMA barrier functions. SKB R-13-40, Svensk Kärnbränslehantering AB.

**Idiart A, Shafei B, 2019.** Modelling of concrete degradation – Hydro-chemical processes. Report for the safety evaluation SE-SFL. R-19-11, Svensk Kärnbränslehantering AB.

**Jacques D, 2009.** Benchmarking of the cement model and detrimental chemical reactions including temperature dependent parameters. Project near surface disposal of category A waste at Dessel. NIROND-TR 2008–30 E, ONDRAF/NIRAS, Belgium.

**Levenspiel O, 1972.** Chemical reaction engineering. 2nd ed. New York: Wiley.

**Lothenbach B, Matschei T, Möschner G, Glasser F P, 2008.** Thermodynamic modelling of the effect of temperature on the hydration and porosity of Portland cement. Cement and Concrete Research 38, 1–18.

**Nardi A, Idiart A, Trinchero P, de Vries L M, Molinero J, 2014.** Interface COMSOL-PHREEQC (iCP), an efficient numerical framework for the solution of coupled multiphysics and geochemistry. Computers & Geosciences 69, 10–21.

**Parkhurst D L, Appelo C A J, 2013.** Description of input and examples for PHREEQC Version 3 – A computer program for speciation, batch-reaction, one-dimensional transport, and inverse geochemical calculations. Techniques and Methods 6–A43, U.S. Geological Survey, U.S. Geological Survey, Denver, Colorado.

**Parkhurst D L, Kipp K L, Charlton S R, 2010.** PHAST version 2: a program for simulating ground-water flow, solute transport, and multicomponent geochemical reactions. Techniques and Methods 6–A35, U.S. Geological Survey, Denver, Colorado.

# Appendix A

## Saturation indices for groundwater

**Table A-1. Saturation indices for meteoric groundwater composition used in the simulations are given in the table below, together with the equilibrium constant of the mineral (log K) and its chemical formula.**

| Mineral | Saturation indices for groundwater | Saturation indices for concrete porewater | Molar volume ($m^3$/kmol) | log K | Dissolution reactions used to calculate solubility products log K |
|---|---|---|---|---|---|
| Brucite | −3.56 | −0.17 | 0.024 | 16.84 | $Mg(OH)2$ |
| Calcite | 0.12 | −0.30 | 0.037 | 1.85 | $CaCO_3 \rightarrow Ca^{2+} - H^+ + HCO^{3-}$ |
| $CSH_{jen}$ | −10.15 | 0.00 | 0.078 | −13.16 | $(CaO)_{1.6667}(SiO_2)(H_2O)_{2.1} \rightarrow 1.6667Ca^{2+} + SiO(OH)_3^- + 2.3333OH^- - 0.5667\ H_2O$ |
| $CSH_{tob2}$ | −3.50 | −0.83 | 0.059 | −8.00 | $(CaO)_{0.8333}\ (SiO_2)(H_2O)_{1.3333} \rightarrow 0.8333Ca^{2+} + SiO(OH)_3^- + 0.6667OH^- - 0.5H_2O$ |
| Ettringite | −20.43 | 0.00 | 0.707 | −44.84 | $Ca_6Al_2(SO_4)_3(OH)_{12}\cdot 26H_2O \rightarrow 6Ca^{2+} + 2Al(OH)_4^- + 3SO_4^{2-} + 4OH^- + 26H_2O$ |
| Gypsum | −2.48 | −1.60 | 0.075 | −4.58 | $CaSO_4\cdot 2H_2O \rightarrow Ca^{2+} + SO_4^{2-} + 2H_2O$ |
| Hemicarboaluminate | −26.22 | −4.14 | 0.285 | −29.12 | $Ca_4Al_2(CO_3)_{0.5}(OH)_{13}\cdot 5.5H_2O \rightarrow 4Ca^{2+} + 2Al(OH)_4^- + 0.5CO_3^{2-} + 5OH^- + 5.5H_2O$ |
| Hydrogarnet OH | −23.24 | −5.43 | 0.150 | −20.84 | $Ca_3Al_2(OH)_{12} \rightarrow 3Ca^{2+} + 2Al(OH)_4^- + 4OH^-$ |
| Hydrogarnet Si | −13.97 | 0.00 | 0.143 | −29.87 | $Ca_3Al_2(SiO_4)_{0.8}(OH)_{8.8} + 2.4H_2O \rightarrow 3Ca^{2+} + + 2Al(OH)_4^- + 0.8\ SiO(OH)_3^- + 3.2OH^-$ |
| Hydrotalcite C | −3.50 | −8.48 | 0.220 | −51.14 | $Mg_4Al_2(OH)_{12}CO_3\cdot 3H_2O \rightarrow 4Mg^{2+} + 2Al(OH)_4^- + CO_3^{2-} + 4OH^- + 3H_2O$ |
| Hydrotalcite OH | −4.43 | 0.00 | 0.220 | −56.02 | $Mg_4Al_2(OH)_{14}\cdot 3H_2O \rightarrow 4Mg^{2+} + 2Al(OH)_4^- + 6OH^- + 3H_2O$ |
| Monocarboaluminate | −20.98 | −3.60 | 0.262 | −31.46 | $Ca_4Al_2(CO_3)(OH)_{12}\cdot 5H_2O \rightarrow 4Ca^{2+} + 2Al(OH)_4^- + CO_3^{2-} + 4OH^- + 5H_2O$ |
| Monosulfoaluminate | −21.91 | −3.21 | 0.309 | −29.24 | $Ca_4Al_2(SO_4)(OH)_{12}\cdot 6H_2O \rightarrow 4Ca^{2+} + 2Al(OH)_4^- + SO_4^{2-} + 4OH^- + 6H_2O$ |
| Portlandite (CH) | −8.98 | 0.00 | 0.033 | 22.81 | $Ca(OH)_2 \rightarrow Ca^{2+} - 2H^+ + 2H_2O$ |
| $SiO_2$ am | −1.17 | −5.98 | 0.089 | 1.48 | $SiO_2 + 1OH^- + 1H_2O \rightarrow SiO(OH)_3^-$ |
| Thaumasite | −9.22 | 0.00 | 0.0332 | −49.36 | $Ca_6(SiO_3)_2(SO_4)_2(CO_3)_2\cdot 30H_2O \rightarrow 6Ca^{2+} + 2H_3SiO_4^- + 2SO_4^{2-} + 2CO_3^{2-} + 2OH^- + 26H_2O$ |

# Appendix B

## Tabulated key parameter results

**Table B-1. pH values time evolution for two fixed points (x=1.4 m and x=2.8 m). Points corresponding to the right boundary of the two control volumes.**

| Time (years) | Inner backfill-outer backfill, x = 1.4 m pH | Outer backfill-waste domain, x = 2.8 m pH |
|---|---|---|
| 0 | 12.9754 | 12.9754 |
| 10000 | 12.5056 | 12.5495 |
| 20000 | 12.4847 | 12.4943 |
| 30000 | 12.4825 | 12.4837 |
| 180000 | 12.3414 | 12.4813 |
| 190000 | 12.3547 | 12.4817 |
| 200000 | 12.3058 | 12.4816 |
| 220000 | 12.2559 | 12.4817 |
| 230000 | 12.1994 | 12.4813 |
| 240000 | 12.2048 | 12.4816 |
| 250000 | 12.1532 | 12.4814 |
| 260000 | 12.1328 | 12.4816 |
| 270000 | 12.1120 | 12.4815 |
| 310000 | 11.8610 | 12.4804 |
| 320000 | 11.8552 | 12.4806 |
| 330000 | 11.6951 | 12.4809 |
| 340000 | 11.2433 | 12.4807 |
| 350000 | 10.9616 | 12.1150 |
| 360000 | 10.7819 | 12.1158 |
| 370000 | 10.6534 | 12.1096 |
| 380000 | 10.6278 | 12.1109 |
| 390000 | 10.6053 | 12.1106 |
| 410000 | 10.5947 | 10.5958 |
| 420000 | 10.5983 | 10.5980 |
| 490000 | 10.6098 | 10.6088 |
| 530000 | 10.6155 | 10.6137 |
| 540000 | 10.6053 | 10.6052 |
| 570000 | 10.6142 | 10.6025 |
| 580000 | 10.4318 | 10.6126 |
| 600000 | 10.4065 | 10.6117 |
| 620000 | 10.4288 | 10.6093 |
| 640000 | 10.4423 | 10.6092 |
| 660000 | 10.4692 | 10.6195 |
| 670000 | 10.4716 | 10.6242 |
| 680000 | 10.4515 | 10.6085 |
| 700000 | 10.4731 | 10.6198 |
| 710000 | 10.4766 | 10.6249 |
| 720000 | 10.4545 | 10.6102 |
| 740000 | 10.4775 | 10.6214 |
| 750000 | 10.4576 | 10.6291 |
| 780000 | 10.4818 | 10.6401 |
| 790000 | 10.4596 | 10.6297 |
| 820000 | 9.6648 | 10.4642 |
| 830000 | 9.6870 | 10.4646 |
| 840000 | 9.7088 | 10.4639 |
| 850000 | 9.4192 | 10.4670 |
| 860000 | 9.4447 | 10.4716 |
| 870000 | 9.3895 | 10.4508 |
| 880000 | 9.4012 | 10.4495 |
| 890000 | 9.2101 | 10.4783 |
| 900000 | 9.1450 | 10.4552 |
| 950000 | 8.8384 | 10.4713 |
| 980000 | 8.7521 | 10.4793 |
| 990000 | 8.7230 | 10.4549 |

**Table B-2. Porosity and effective diffusion coefficient representative values for inner and outer backfills. Values tabulated for each leaching event.**

| Time (years) | Porosity outer backfill | Porosity inner backfill | $D_{eff}$ ($m^2/s$) outer backfill | $D_{eff}$ ($m^2/s$) inner backfill | Leaching event |
|---|---|---|---|---|---|
| 0 | 0.11 | 0.11 | 3.5E−12 | 3.5E−12 | Initial values |
| 170 000 | 0.18 | 0.11 | 1.5E−11 | 3.71E−12 | CH in outer b |
| 390 000 | - | 0.19 | - | 1.29E−11 | CH in inner b |
| 780 000 | 0.28 | 0.20 | 3.74E−11 | 1.44E−11 | C-S-H in outer b |
| 1 000 000 | 0.29 | 0.24 | 3.86E−11 | 2.27E−11 | Final values |

# Appendix C

## Solute transport characterization

The main objectives of this appendix are to:

1. Give a more in depth analysis of solute transport processes in the 1D setup presented in the report
2. Verify the soundness of the model numerical setup,
3. Study some mineralogical assemblage details, and
4. Assess the effect of the modified Kozeny-Carman relation between porosity and hydraulic conductivity.

To this end, several auxiliary models are presented below and compared to the 1D reactive transport model detailed in the report:

- The original 1D iCP reactive transport model has been recalculated with different time stepping, boundary water chemical setup or hydraulic conductivity parameter definition.
- A conservative transport model has been set up in Comsol Multiphysics. No chemical reactions are included. Geometry, mesh and initial transport properties are equivalent to those of the complete model. Porosity, effective diffusion coefficient and permeability are constant throughout the simulation. The time step size is also constant (10 years) and the total study time reaches 1 000 years. Tracer concentration is fixed in 0.1 mol/m$^3$ in the left boundary, while its initial value in the model domain is set to 0.001 mol/m$^3$. An outflow condition is prescribed in the right boundary.
- The reactive transport model presented in the report has been repeated for this appendix using the software PHAST (Parkhurst et al. 2010). This model has constant transport properties and no porosity changes or coupling effects. Thus, in this case there are no changes in the contribution of advection and diffusion over time.

### C.1 Contribution of diffusion and advection to solute transport

A conservative transport model is implemented in Comsol and used to study the effect of changing the initial effective diffusion coefficient and Darcy flow velocity on solute transport. The goal is to illustrate the contribution of advective and diffusive mass fluxes to solute transport. First, using the same Darcy flow as the 1D reactive transport model ($1.03 \times 10^{-11}$ m/s), several simulations were performed with different values of effective diffusion coefficient ($D_{eff}$).

Figure 7-13 shows the results of these four simulations in terms of tracer concentration 1D profiles. The results clearly show that the contribution of diffusive fluxes to solute transport is non-negligible. The value for intact concrete ($D_{eff} = 3.5 \times 10^{-12}$ m$^2$/s) leads to a less advective-dominated transport regime, as compared results for lower diffusivities. The effect of increasing the diffusion coefficient from $3.5 \times 10^{-12}$ to $3.5 \times 10^{-11}$ m$^2$/s) is a significantly greater penetration of the tracer profile.

In addition, three simulations with different advective fluxes are compared, with the same $D_{eff} = 3.5 \times 10^{-12}$ m$^2$/s. Figure 7-13b shows the results these three simulations. One of the cases considers a zero Darcy flow, corresponding to a pure diffusion setup. Again, the results show that the impact of diffusion on the tracer profiles is important.

As shown in Chapter 5, the Péclet number of the concrete backfill ranges between 50 and 150, indicating that the model is advective transport is dominating over diffusive transport throughout the simulation. However, diffusive transport still plays an important role. Figure C-2 shows the results of the 1D reactive transport model in terms of local Péclet numbers, calculated as:

$$Pe_{local} = \frac{q\Delta x}{\varphi D_e} \qquad \text{(C-1)}$$

where $\Delta x$ (m) is the finite element size (0.1 m in this setup), and $\varphi$ and $D_e$ are the porosity and effective diffusion coefficient at the finite element level. It may be observed that the contribution of diffusion to solute transport is more important in the degraded part of the backfill. Important differences are observed between the degraded and the non-degraded regions. The reason for these differences is that while the Darcy flow is homogeneous along the entire backfill thickness, the diffusivity and porosity are much larger in the degraded regions than in the unleached regions.

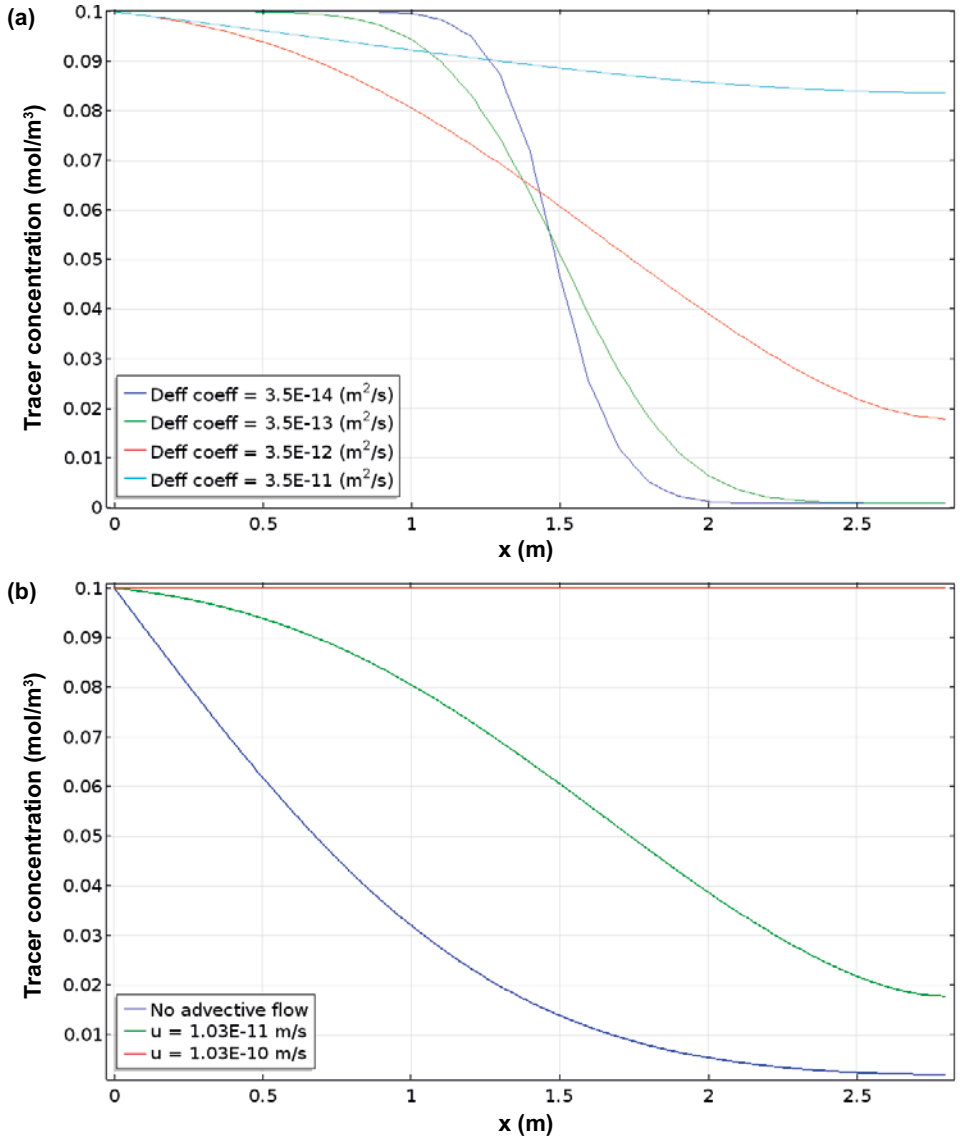


***Figure C-1.*** *Comsol conservative transport model results. Tracer concentration spatial distribution along the concrete backfill after 500 years. (a) Results for 4 different effective diffusion coefficients with the original advective flow. (b) Results for 3 different advective flow conditions with the original effective diffusion coefficient.*

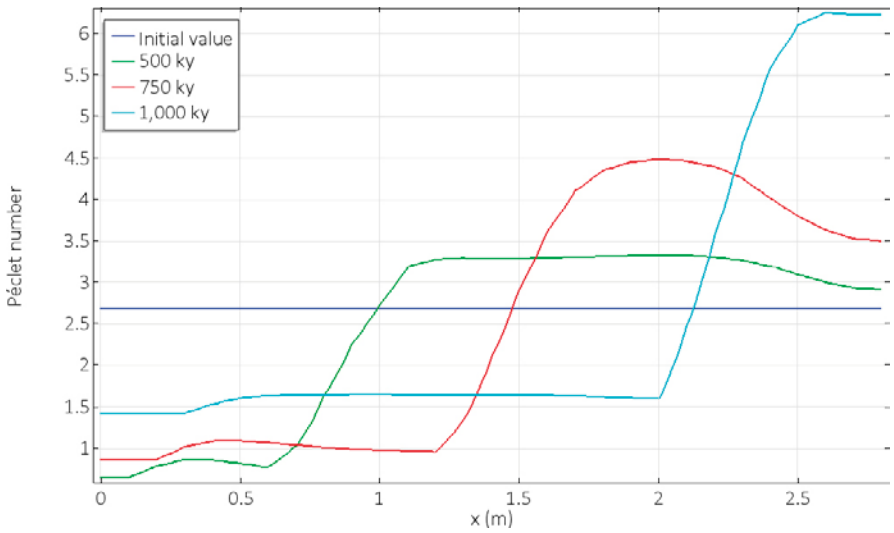


***Figure C-2.*** *Results of the 1D reactive transport model: local Péclet number spatial distribution at different times.*

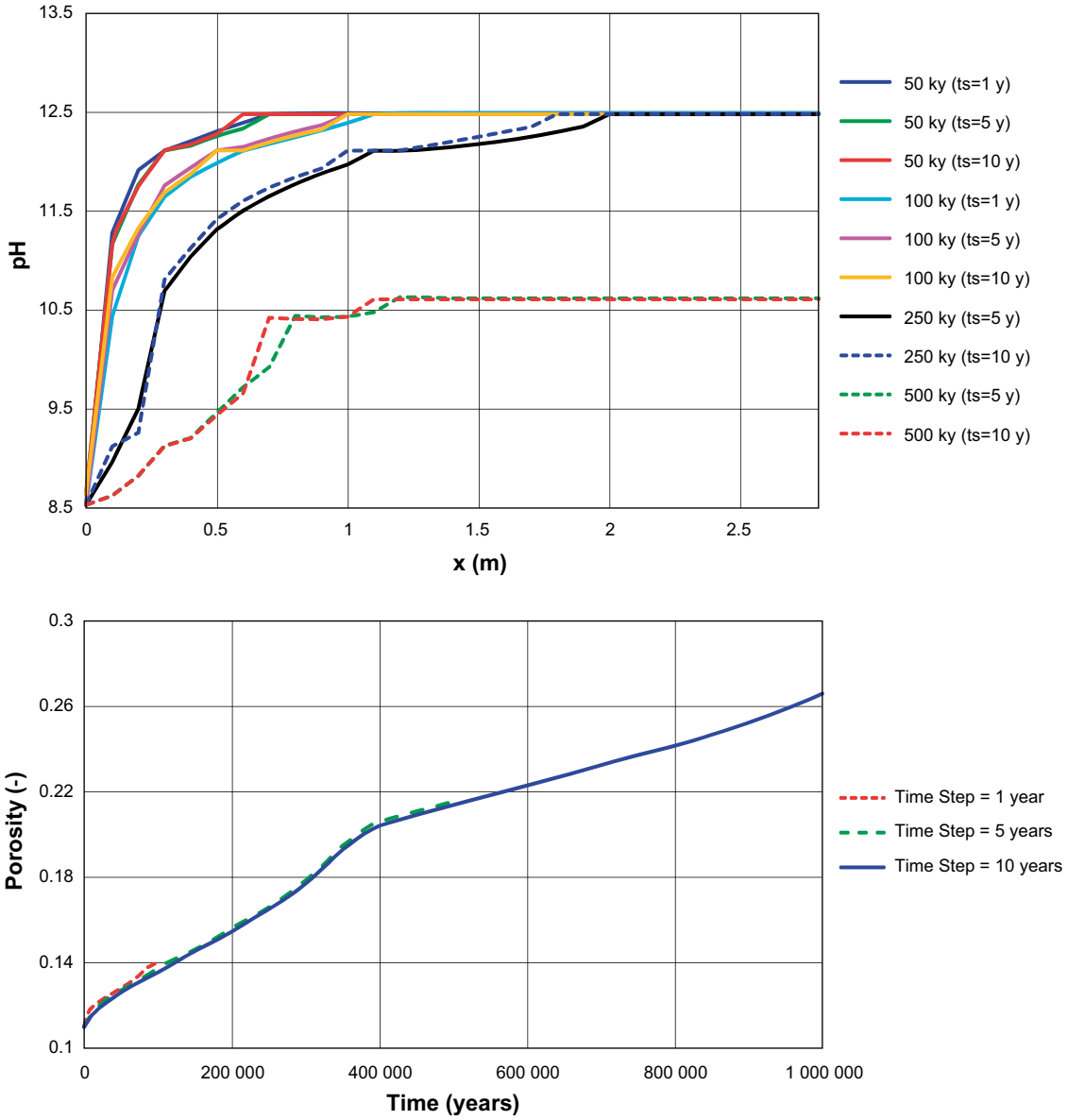


***Figure C-3.*** *Comparison between different time step sizes (1, 5 and 10 years) of the 1D reactive transport model: pH spatial distribution profiles at different times (top) and integrated value of porosity for the concrete backfill thickness (bottom).*

## C.2 Numerical setup verification

The effect of temporal discretization used in the 1D reactive transport model has been assessed by means of additional simulations with smaller time step sizes. The results in Chapter 6 are obtained with a time step of 10 years. Results have also been c using a time step size of 1 and 5 years, with shorter simulation times (100 000 time steps). Results from the three models, in terms of pH and porosity, are compared in Figure C-3. It may be observed that similar results are obtained using different time step sizes.

The impact of spatial discretization on solute transport results has also been analyzed. The Comsol model for transport of a conservative tracer described above is used to study the sensitivity of the results to mesh refinement. The results of the model with a spatial discretization of 0.1 m (as in Chapter 5) are compared with those of a model with a discretization of 0.01 m in Figure C-4. It can be observed that the results are equivalent.

## C.3 Chemical setup verification

The 1D reactive transport model in iCP has also been implemented in PHAST (Parkhurst et al. 2010) for comparison purposes. The effect of porosity feedback on transport properties is not included in the PHAST simulation. The impact of this feature, which is considered in the iCP simulation, is assessed here. The results in terms of pH and portlandite and C-S-H gels concentrations are presented in Figure C-5. First, it can be observed that degradation is predicted to be much slower if porosity feedback is not considered. For instance, complete portlandite depletion from the concrete backfill occurs after ~750 000 years in this model, while results in Chapter 6 indicate a much shorter time (~350 000 years). This expected result is due to the increasing velocity, porosity, and diffusion coefficient in the fully coupled case (Chapter 6). It is also shown that the time period between complete portlandite dissolution and C-S-H decalcification at a given point increases with the distance to the groundwater source, as opposed to the more complex behaviour of the coupled case (Chapter 6).

The evolution of the portlandite dissolution depth over time obtained using the uncoupled setup in PHAST is compared to the iCP model (Chapter 6) in Figure C-6. The SCM estimates using the degraded and intact values of the effective diffusion coefficients are also included for comparison. It may be observed that the influence of advection is also dominating solute transport and degradation in the uncoupled case.

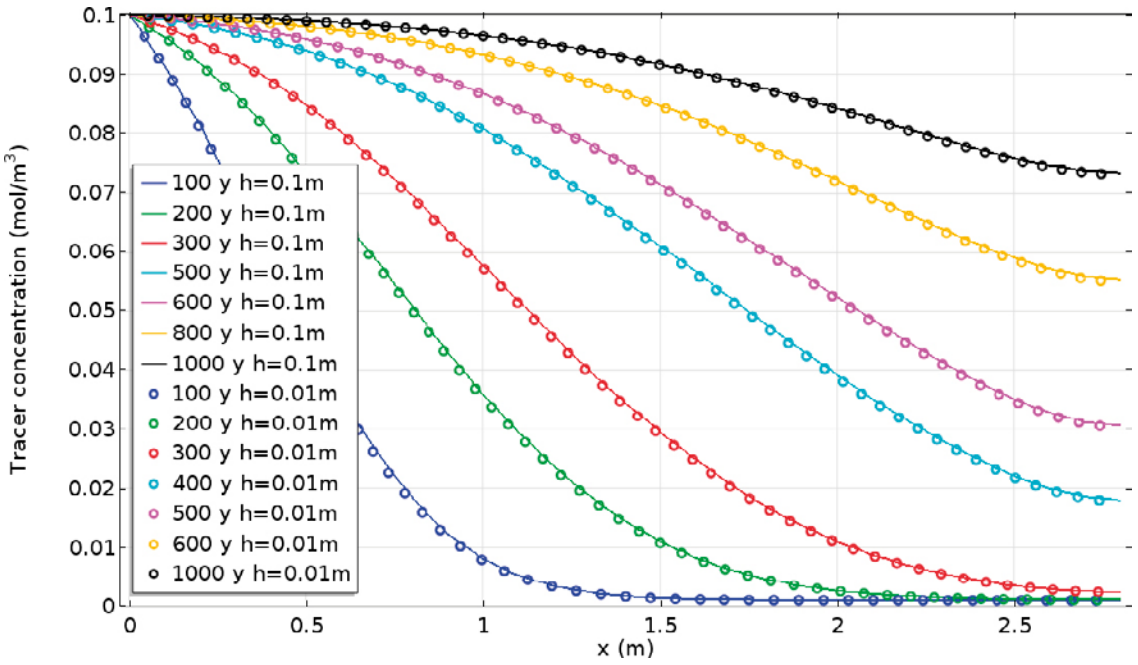


***Figure C-4.*** *Results of the transport of a conservative tracer in Comsol using two different spatial discretizations (0.01 and 0.1 m): concentration spatial distribution along the concrete backfill at different times. Solid lines correspond to the original mesh size and markers represent the solution for a 10 times finer spatial discretization.*

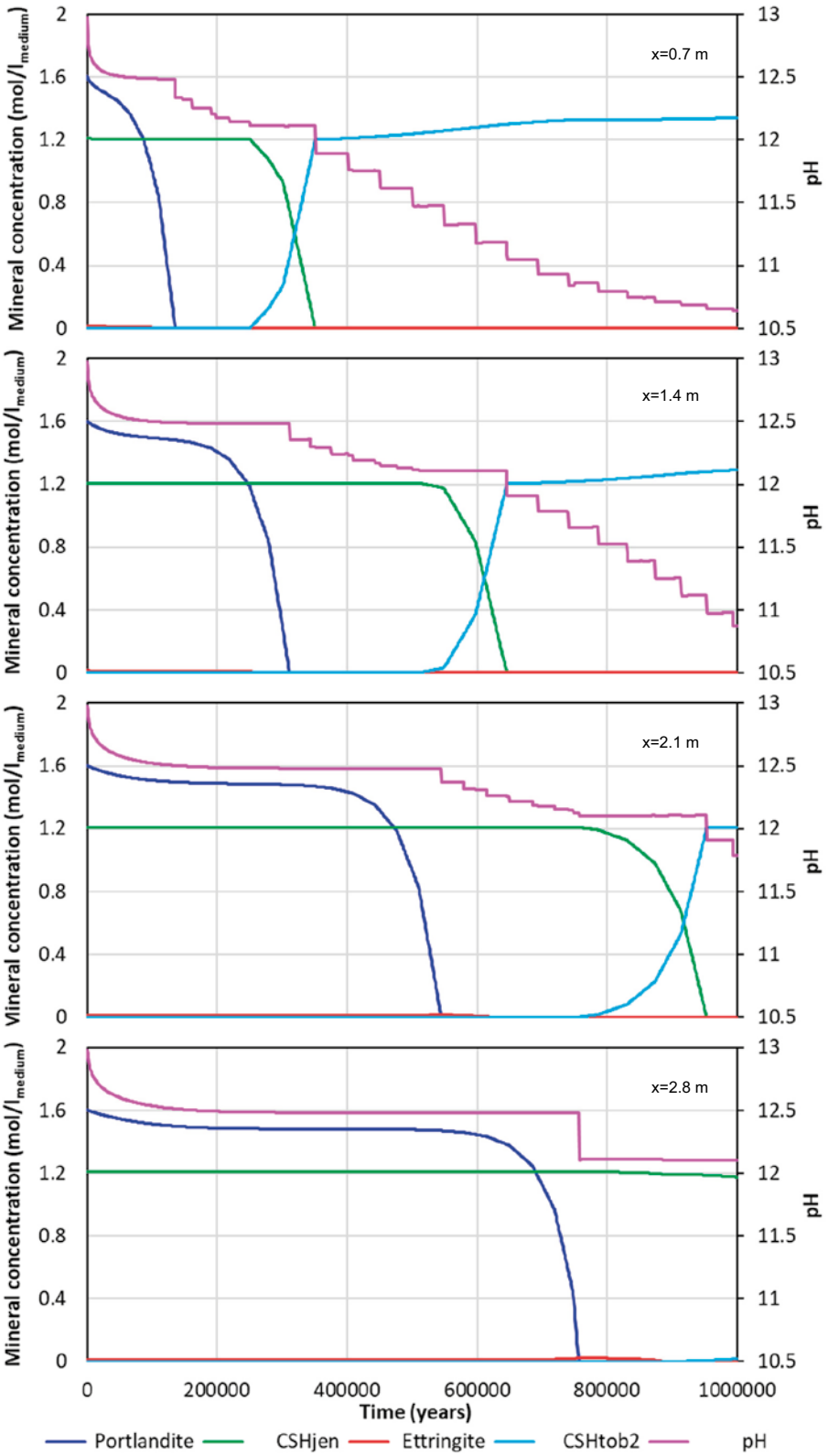


***Figure C-5.*** *Evolution of pH and portlandite and C-S-H gels concentrations at different points of the concrete backfill: 0.7, 1.4, 2.1 and 2.8 m (from top to bottom).*

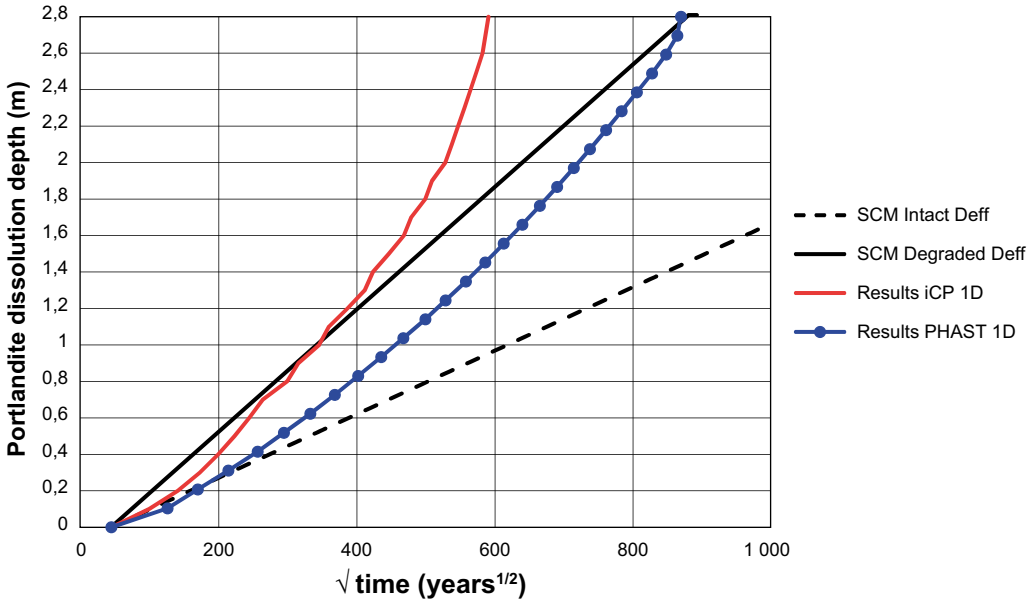


***Figure C-6.*** *Comparison of portlandite dissolution depth evolution obtained with different models: 1D reactive transport models using iCP (in red, with porosity feedback) and PHAST (in blue, no porosity feedback) and the SCM results considering the degraded (black solid line) and intact diffusion coefficients (black dotted line).*

## C.4 Relation between porosity and hydraulic conductivity

The definition of the relation between hydraulic conductivity and porosity is subject to a high degree of uncertainty due to lack of sufficient experimental data. The Kozeny-Carman equation (Carman 1937) has been used in the work presented in this report. In this appendix section, the modified Kozeny-Carman relation (see for instance Idiart and Shafei 2019) is assessed. The main difference of this relation with respect to the classical Kozeny-Carman equation is that it assumes that the hydraulic conductivity ranges between the initial value of the intact concrete and a final state where all cement minerals have been depleted, leaving a skeleton of the initial ballast material that controls the conductivity. Thus, dramatic changes in hydraulic conductivity are calculated when porosity reaches its maximum value of 0.3. Figure C-7 presents the two relations between porosity and hydraulic conductivity.

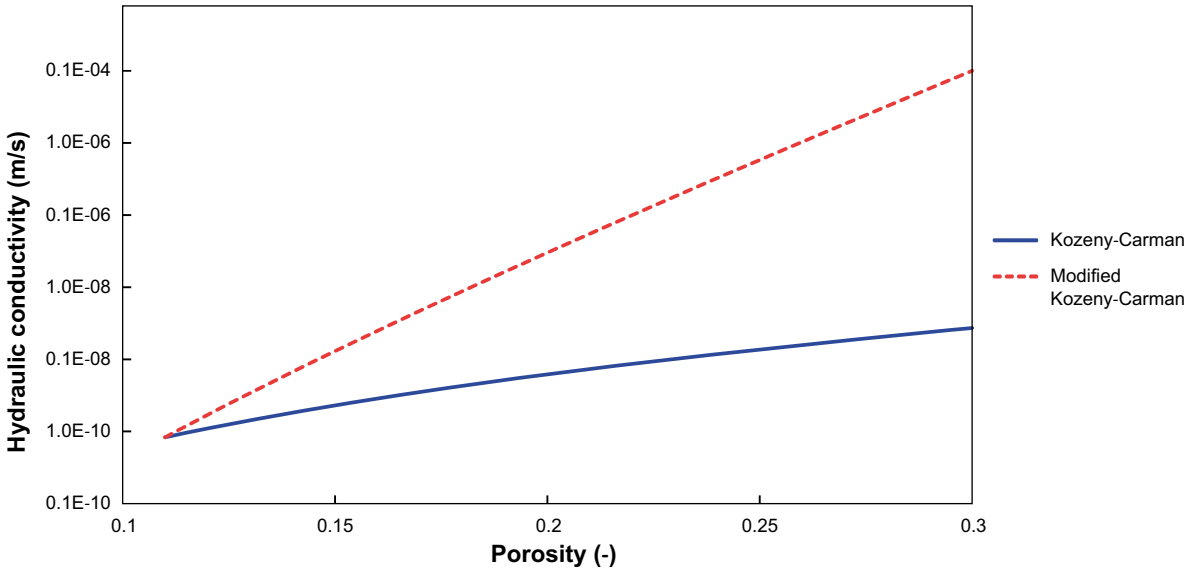


***Figure C-7.*** *Hydraulic conductivity values (m/s) calculated for each porosity value (-). Representation of Kozeny-Carman and modified Kozeny-Carman laws.*

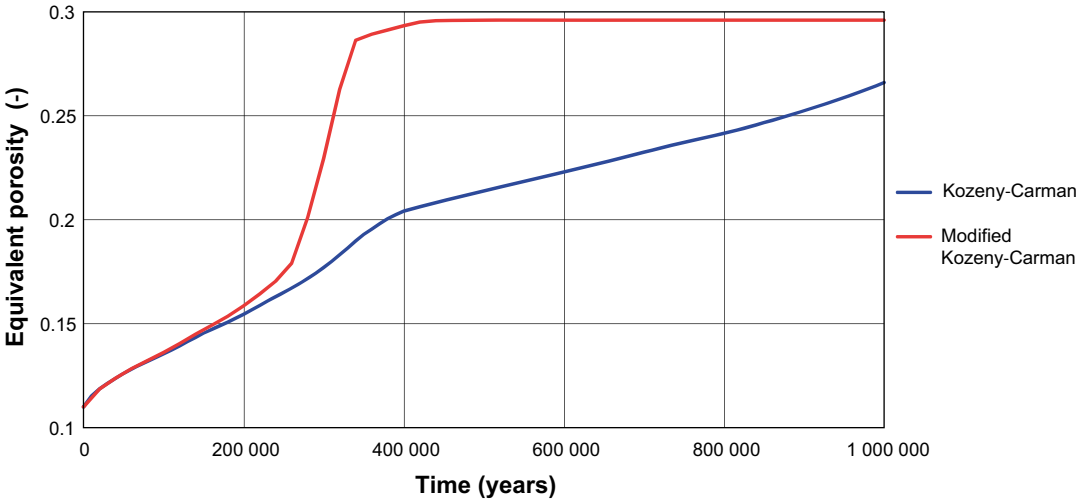


***Figure C-8.*** *Equivalent porosity for the whole concrete backfill temporal variation. Comparison between iCP RTM models set up with the Kozeny-Carman and modified Kozeny-Carman laws.*

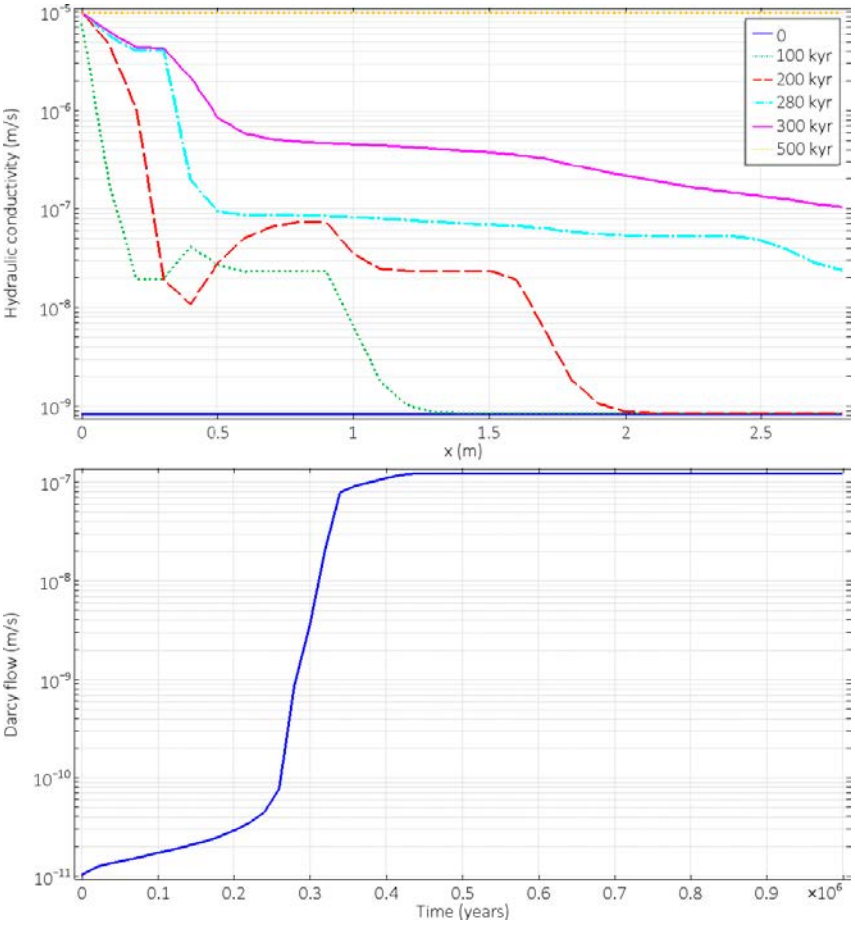


***Figure C-9.*** *Hydraulic conductivity (m/s) spatial distribution at different times (top) and evolution of the Darcy flow velocity (m/s) in the concrete backfill as a function of time (bottom).*

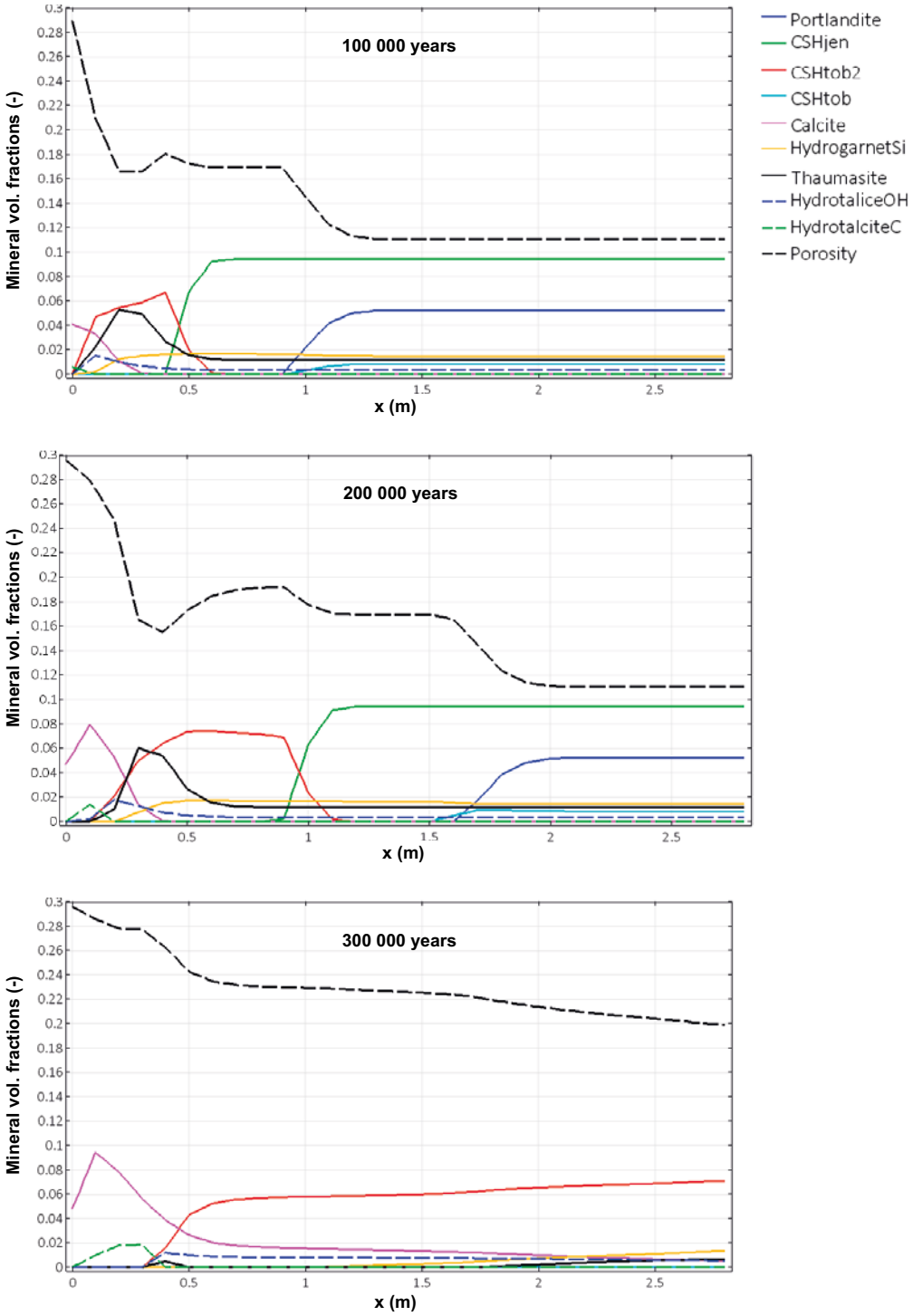


***Figure C-10.*** *Mineral volume fractions at different times, spatial distribution in the concrete backfill (length in m).*

The 1D reactive transport simulation has been repeated using the modified Kozeny-Carman equation. In this case, a much faster degradation is expected, given the constant head gradient boundary condition, with advective transport largely dominating solute transport. The differences in the results in terms of averaged porosity values of the concrete backfill are presented in Figure C-8. The use of the modified Kozeny-Carman relation leads to a fully degraded concrete backfill after 450 000 years.

The evolution of the hydraulic conductivity and the Darcy velocity is shown in Figure C-9. The values of hydraulic conductivity for the degraded concrete are in this case orders of magnitude higher than those given by the Kozeny-Carman relation for the same porosity value. Between 200 000 and 300 000 years, the hydraulic conductivity of the entire thickness of the concrete backfill increases. At this point, the rate of increase of Darcy velocities increases sharply. This increase coincides with the rate of degradation of the cement hydrates (Figure C-10) and the increase in the rate of porosity changes (Figure C-8). Between 200 000 and 300 000 years, portlandite is completely leached, while CSHjen is fully replaced by CSHtob2 (C-S-H gel decalcification), as shown in Figure C-10.

The results obtained when using the modified Kozeny-Carman relation should be analysed with some caution. This is because there are some limitations related to the 1D setup used in this study. The main limitation is that the use of a constant hydraulic head gradient boundary condition leads to a linear increase of the Darcy flow with the equivalent conductivity of the backfill. Since the latter increases by orders of magnitude with the modified Kozeny-Carman relation, so does the groundwater velocity.

It is known from the hydrogeological models of SFL, however, that above a certain threshold value of the concrete hydraulic conductivity, the host rock that acts as a hydraulic barrier and limits the inflow of groundwater to the vault (Abarca et al. 2016, 2019). This is shown in Figure C-11. The graph also shows that the flow entering the vault is not linearly proportional to the hydraulic conductivity of the concrete backfill. An increase of more than 2 orders of the concrete hydraulic conductivity leads to an average vault flow that is only ~20 times higher.

Moreover, in the 1D setup there cannot be any redirection of flow, as observed in 2D simulations (Idiart and Shafei 2019). In summary, the 1D model using the modified Kozeny-Carman relation will produce very aggressive degradation conditions. Nonetheless, it can be considered as a bounding case to gain insight about how fast concrete degradation can occur.

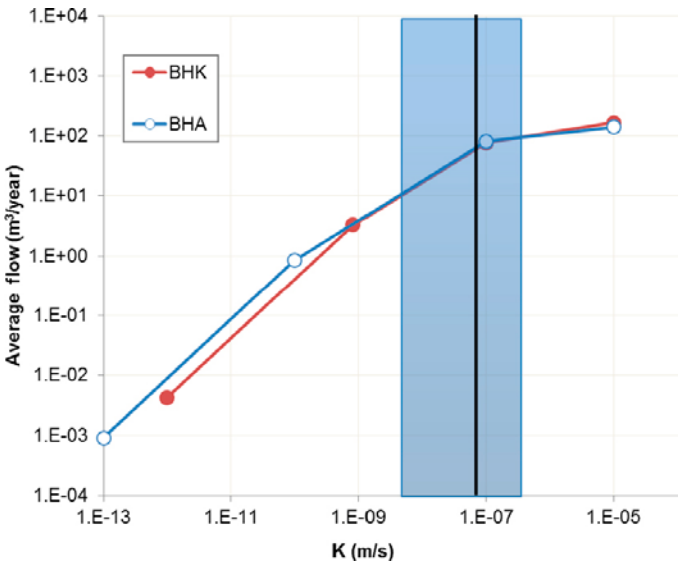


***Figure C-11.*** *Average flows through the BHA and BHK vaults considering different hydraulic conductivities of the backfills (from Abarca et al. 2016). The blue zone indicates the range of hydraulic conductivities in the rock at a depth of 500 m. The black line indicates the average hydraulic conductivity of the rock at repository depth.*

Arkitektkopia AB, Bromma, 2019

SKB is responsible for managing spent nuclear fuel and radioactive waste produced by the Swedish nuclear power plants such that man and the environment are protected in the near and distant future.

**skb.se**